

THE OPTIMIZATION OF GOLD COATED IRON NANOPARTICLE SYNTHESIS

METHODS

by

Mark Riggs, B.S., B.S.

A thesis submitted to the Graduate Council of
Texas State University in partial fulfillment
of the requirements for the degree of
Master of Science
with a Major in Chemistry
August 2014

Committee Members:

Gary Beall

Shannon Weigum

Clois Powell

COPYRIGHT

by

Mark Riggs

2014

FAIR USE AND AUTHOR'S PERMISSION STATEMENT

Fair Use

This work is protected by the Copyright Laws of the United States (Public Law 94-553, section 107). Consistent with fair use as defined in the Copyright Laws, brief quotations from this material are allowed with proper acknowledgment. Use of this material for financial gain without the author's express written permission is not allowed.

Duplication Permission

As the copyright holder of this work I, Mark Riggs, authorize duplication of this work, in whole or in part, for educational or scholarly purposes only.

DEDICATION

I dedicate this to my wife, Melissa. Her constant support and encouragement were nothing short of heroic. Careful and delicate allocation of my focus became ever-increasing in importance throughout the progression of this research, primarily due to the birth of my beautiful daughter, Olivia Marie, on February 4th of 2014. My daughter's arrival impacted my perception in ways I couldn't have fully understood prior to that wonderful moment. I will be forever indebted to Melissa for showing me how blessed I am, enabling me to live a better life than I could have conceived, and providing never-ending assistance with caring for our daughter. She truly took it upon herself to ensure that I maintained my sanity while pursuing my M.S. in Chemistry. I love you Melissa, and this accomplishment was so dependent on your help, that your name should be right under the title.

ACKNOWLEDGEMENTS

The collection of data found in this thesis would not have been possible if it weren't for the ENTIRE chemistry department at Texas State University. I consider myself very lucky to attend a university where the priority is the furthering of one's education and not the furthering of one's own career. Every member of the faculty has helped me either directly or indirectly at several points during my tenure as a graduate student. The assistance provided ranged from helping me to locate some chemical reagents critical to my research, to teaching me how to use instrumentation I was unfamiliar with. Dr. Gary Beall, my research advisor, has been an asset that cannot be over-stated. His abundance of experience and technical expertise in the field of material science is staggering. He was an ever-present watchman for my laboratory endeavors, always ready to answer questions that I hadn't even formulated yet. This research project would not have been funded if it weren't for my other research advisor, Dr. Shannon Weigum. I am so thankful for being given the opportunity to work on her research project, and she was always willing to give me advice and extended me access to high-quality laboratory resources. Dr. Clois Powell, the third member of my thesis committee, was constantly helping locate information for me relative to the project. He is so knowledgeable and was always willing to help me when I had any questions. Additionally, the members of my research group have been a fantastic source of assistance and guidance. Brandon Henderson deserves special recognition in this regard,

for not only sharing his in-depth knowledge of chemistry, but for his willingness to put his work aside to help someone who is clearly struggling with theirs (which was frequently me). That manner of selflessness is awe-inspiring and is a quality I hope all future scientists will aspire towards. Some time ago, our country's academic merits were measured by the scientific community's accomplishments as a whole instead of by any one individual's deeds, and great things were discovered. I believe we can embody that mentality again, and strive for deeper understanding instead of early retirement.

TABLE OF CONTENTS

	Page
ACKNOWLEDGEMENTS.....	v
LIST OF FIGURES	ix
LIST OF ABBREVIATIONS.....	xi
ABSTRACT.....	xii
CHAPTER	
I. INTRODUCTION.....	1
II. CURRENT GOLD-COATED NANOPARTICLE SYNTHESIS METHODS..	4
“Ground-Up” Synthesis Methods	5
Enthalpy-Driven Gold Reduction onto Metals	5
Co-Precipitation Method.....	7
Micellar-Based Reduction	8
“Top-Down” Synthesis Methods	10
Electroless Gold Plating onto Nanobeads.....	10
Reduction of Gold onto Iron Nanospheres and Nanorods	11
Magnetization of Superatomic Gold Clusters.....	12
Assigning the Preferred Synthesis Method.....	13
Optimizing the Preferred Synthesis Method.....	15
III. EXPERIMENTAL METHODS.....	18
Preparation of Micellar Solutions	18
Functionalization of the Nanoparticle Surface	20
Ion Exchange Treatment.....	21
Light Scattering Measurements	21
SEM Analysis	22
UV-Vis Spectroscopy	22
Magnetic Hysteresis Characterization	23
TGA Trials	23
IV. RESULTS AND DISCUSSION.....	24

Evaluation of Different Micelle Sizes.....	24
Dynamic Light Scattering	24
Nanoparticle Product Characterization	25
Dynamic Light Scattering.....	25
SEM Analysis	28
UV-Vis Absorbance.....	33
Magnetic Hysteresis Characterization	35
TGA Trials	37
A Novel Approach for Targeted-Gold Reduction	39
Iron Reduction of Aqueous Gold	39
V. CONCLUSIONS.....	42
APPENDIX	44
REFERENCES	49

LIST OF FIGURES

Figure	Page
1. Inverse Micelle Diagram.....	4
2. DLS Data for 20 Molar Ratio Inverse Micelle	24
3. Inverse Micelle Sizes	25
4. Colloidal Gold Particle Sizes	26
5. DLS of 20 Molar Ratio Fe@Au Product	27
6. SEM Image of 8 Molar Ratio Fe@Au Product.....	28
7. EDS Spectrum of 8 Molar Ratio Fe@Au Product.....	29
8. SEM Image of 20 Molar Ratio Fe@Au Product	30
9. EDS of 20 Molar Ratio Fe@Au Product	30
10. SEM Image of 20 Molar Ratio Iron Oxide Product.....	31
11. EDS of 20 Molar Ratio Iron Oxide Product	32
12. EDS of Silicon Oxide Substrate.....	32
13. UV-Vis of Supernatant versus Gold Colloid	34
14. UV-Vis of Fe@Au versus Iron Oxide Product.....	34
15. Magnetic Hysteresis Loop of Iron Oxide Product	36
16. Magnetic Hysteresis Loop of Fe@Au Product.....	36
17. TGA of 20 Molar Ratio Fe@Au Product.....	37
18. TGA of 20 Molar Ratio CT-Peg Fe@Au.....	38

19. TGA of 20 Molar Ratio Iron Oxide Product.....	39
20. Image of Unoxidized and Oxidized Iron from Novel Gold Reduction Approach	40
21. Image of Novel Gold Reduction Approach Product.....	41

LIST OF ABBREVIATIONS

Abbreviation	Description
°C	Degrees celsius
cm	Centimeters
cm ⁻¹	Reciprocal centimeters (wavenumbers)
CTAB	Cetyltrimethylammonium bromide
CT-Peg	Carboxy thiol polyethylene glycol
EDL	Electrical double-layer
Fe@Au	Gold-coated iron
K	Kelvin
nm	Nanometers
PEG	Polyethylene glycol
SEM	Scanning electron microscopy
TEM	Transmission electron microscopy
DLS	Dynamic light scattering
XPS	X-ray photoelectron spectroscopy
XRD	X-ray diffraction
UV-Vis	Ultraviolet-visible

ABSTRACT

The field of nanomedicine is rapidly growing as the applications of incorporating micro-structured systems into treatment and diagnosis of diseases are being discovered and refined. A “bottom-up” approach to building molecular networks is becoming more common with the increase in available methods that allow for utilization of self-assembly or ordered chemistry at the particle level. Biosensors are medical devices that have employed such systems, and the biosensor market is on the rise as the focus of patient evaluation shifts to point-of-care diagnosis. Successful implementation of these structures into a biosensor is not simple, since reproducibility and sensitivity are paramount in such devices. Those characteristics are contingent on the use of materials that are highly consistent, and tailor-made for a specific biosensor analysis.

Among the materials frequently employed in the fabrication of nanoparticle systems, gold is one of the most popular. Gold has a defined affinity for sulfur, which gives a gold surface the potential for functionalization if a thiolated ligand is used. However gold is rare and costly, and cannot be used frivolously when designing a synthesis method for gold nanoparticle production that is also scalable. Therefore it is desirable to identify and optimize the best synthesis method for this task.

In this paper, an approach is taken to optimize the best-suited method for synthesizing gold-coated iron nanoparticles. The gold coating provides a means to functionalize the nanoparticle for use in a large variety of biosensors, and the magnetic

nature of the particles allow for concentration of analytes in a sample, which improves inherent biosensor sensitivity. Resulting products of this “modified synthesis” were analyzed and evaluated using characterization methods such as scanning electron microscopy, ultraviolet-visible spectroscopy, and vibrating scanning magnetization. Improvements in particle size control and reduced use of expensive reagents were obtained. The nanoparticles produced did not meet the necessary size variance, particle dispersity, and coating uniformity required for implementation in a current biosensor process.

CHAPTER I

INTRODUCTION

The formation of multi-component nanoparticles has been a topic of discussion in journals over the last decade, because particles of this nature can be engineered to accomplish specific duties. Incorporation of desirable properties from multiple materials can lead to a “smart” particle that is multifunctional. One approach to creating these types of particles is through the stepwise formation of a bi-layered particle, which is frequently referred to as a “core-shell” structure.

Gold is a frequently used component in these types of nanoparticles because gold has a well-documented affinity for binding with a sulfur-containing molecule. The advantage of this affinity allows for unique and ordered chemistry to be induced between thiolated conjugates and gold surfaces. These conjugates are commonly alkyl chains containing a functional end group, such as an amine or a carboxylic acid, which also acts as a binding site for additional conjugation. Another attractive quality inherent to gold is its minimal health risk to human physiology in low doses.¹

The incorporation of gold into diagnostic nanomedicine has shown great potential, specifically in applications using imaging, targeting, and therapeutic tools.² In order to gain a level of control over the gold surface, a core composed of a magnetic material enables the user to direct movement of the particles through use of an external magnetic field.³ The type of material comprising the magnetic core is superparamagnetic. A particle that responds strongly to an applied magnetic field, but doesn't remain magnetized in the absence of the magnetic field, is ideal for biomedical applications.³

This allows for quick concentration and separation of the particles from sample solutions, making these particles ideal for nanomedicine applications for point-of-care diagnosis.³

Potential applications for gold-coated magnetic nanoparticles are extensive. For example, untreated colloidal gold nanoparticles are employed in biological imaging, drug delivery, photothermal ablation, and as biosensor components.² Improvements to nanomedicine efficacy and target accuracy for magnetic gold versus non-magnetic gold are significant, so a reliable means to produce particles of this nature is sought after.

Verification that gold-coated magnetic nanoparticles can be produced and are stable has been established by several different research groups.⁴⁻⁹ The gold-coated magnetic nanoparticles are frequently studied for their properties and rarely used in biomedicine applications. Formation of uniform particles, removal of residual surfactant, and effective particle stabilization are all examples of difficulties facing researchers synthesizing magnetic gold nanoparticles.^{4,10}

To achieve results consistent with the level of quality available from commercial nanoparticle producers, current core-shell synthesis methods were compared and contrasted, and a preferred method selected. Changes that could be made to the process that would improve output, reduce cost, or reduce size distribution range were identified, and implemented in an attempt to form consistent gold-coated iron (Fe@Au) nanoparticles that were capable of operating as a functional biomedicine component. This thesis summarizes the properties of gold-coated magnetic nanoparticles made using current synthesis methods, and describes the criteria for assigning a preferred synthesis method. The preferred method was modified to produce large particles and localize gold

shell reduction to the iron particle surface, and the results of that modified synthesis are characterized and discussed.

CHAPTER II

CURRENT GOLD-COATED NANOPARTICLE SYNTHESIS METHODS

There are many different approaches to synthesizing this class of nanoparticles, but two are most commonly used in practice. The first method is based on a “ground-up” synthesis approach, where the metallic core is reduced or precipitated in solution, and the gold shell is grown at the particle surface.⁴⁻⁶ If the metal core is being formed via reduction, this is performed in an inverse micelle to control the particle size (Figure 1).⁶ This emulsion is formed because the polar head group of a surfactant and co-surfactant surround water, while the hydrophobic tail group of the surfactant interacts with the organic phase of the solution. Common surfactants used include tetramethylammonium hydroxide and cetyltrimethylammonium bromide (CTAB), and some examples of reducing agents used are sodium borohydride and lithium aluminum hydride. If the

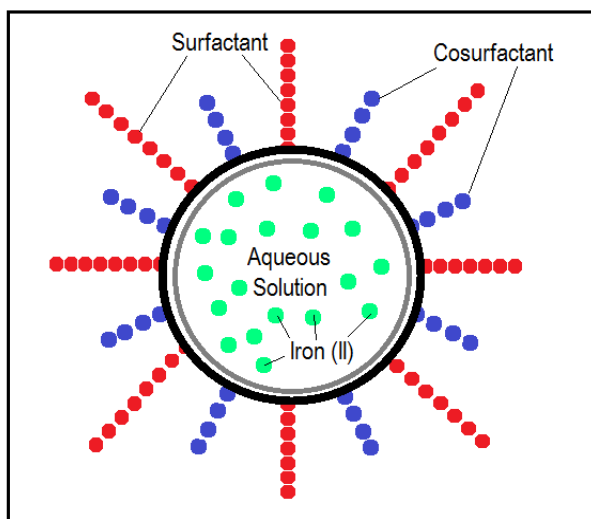


Figure 1: Inverse Micelle Diagram. A diagram depicting the formation of an inverse micelle in an organic continuous phase. The aqueous droplet is stabilized with the presence of a co-surfactant.

metal core is being formed via precipitation in an aqueous medium, the salt metal conjugate is dissolved in an acidic solution then precipitated out of solution by increasing the pH.⁵ If the metal core is being formed via precipitation in an organic solution, the solution is heated and stirred to disassociate the ligand-metal bonds, forming metal nanoparticles.⁴ Due to the difficult nature of attempting to control Ostwald-ripening in aqueous solvents, the reduction of metal atoms in the inverse micelle is the preferred approach, and is more frequently utilized.¹¹ The second method consists of gold shell formation on commercially purchased magnetic nanoparticles, and is referred to as the “top-down” synthesis approach.

“GROUND-UP” SYNTHESIS METHODS

Enthalpy-Driven Gold Reduction onto Metals

Robinson *et al.* prepared iron oxide and cobalt nanoparticles in an organic solvent both with and without gold coatings.⁴ The cobalt nanoparticles were precipitated from cobalt carbonyl dissolved in anhydrous toluene, which was combined with sodium sulfosuccinate and stirred under inert gas protection at 110 °C. The increase of enthalpic energy allows for the expulsion of the carbon monoxide ligands from the cobalt complexes, and the sodium sulfosuccinate acts as a capping agent to prevent aggregation of the cobalt particles.⁴ To add a gold coating to these particles, chloroauric acid trihydrate was added to a mixture of the sodium sulfosuccinate capped cobalt particles at

85 °C.⁴ Oleylamine was also added at the same time as the chloroauric acid to assist with the incorporation of a hydrated product into an organic solution.⁶

The iron oxide nanoparticles were formed using iron acetylacetonate dissolved in phenyl ether with oleic acid.⁴ The solution was then refluxed for several hours, again under nitrogen. The gold coating was introduced to these nanoparticles in a similar fashion as described above, however the gold source was not hydrated. Gold was provided using gold acetate. The temperature of the reaction here was 185 °C, implying that there is a greater activation energy for gold reduction in gold acetate as opposed to reduction of gold in chloroauric acid, which can be formed at ambient temperatures.

Gold-coated and uncoated cobalt and iron particles produced by the Robinson group were compared using Transmission Electron Microscopy (TEM) and Dynamic Light Scattering (DLS) data. The results showed a very narrow size distribution for both sets of nanoparticles. It should be noted that the difference in particle diameter between the treated cobalt particles and untreated cobalt particles was nearly negligible. The iron nanoparticles, comparatively, showed an improved level of gold reduction at the particle surface, with a 37% increase in particle size.⁴ This might be attributed to the higher level of reduction potential in iron atoms versus cobalt atoms, or because the gold source for the cobalt coating process was organic and slower to reduce in an aprotic environment.¹³

A low blocking temperature was discovered during magnetic characterization of iron oxide nanoparticles and their gold-coated counterparts. The blocking temperature is the temperature at which the magnetization fluctuations of the particle no longer occur rapidly (resulting in a net magnetic moment of zero), and particles instead act ferromagnetically and retain magnetization from an applied magnetic field. The larger the

retained magnetization is of a superparamagnetic material below its blocking temperature, the more susceptible the material is to manipulation from an applied external magnetic field.³ The Zero Field-Cooled (ZFC) and Field-Cooled (FC) results were 15 Kelvin (K) and 29 K for uncoated and coated particles, respectively. The coercivities were 90 Oersted (Oe) and 260 Oe at 5 K. They postulated that the increase in blocking temperature and coercivity were due to the increase in diameter from uncoated to coated nanoparticles, which would lead to a less effective coupling of the core magnetic dipoles.¹⁴ The particles formed using this method had a narrow size distribution, but required extended periods of refluxing, and produced small nanoparticles.

Co-Precipitation Method

The co-precipitation method for iron oxide formation was demonstrated by Wagstaff *et al.* in their paper on tumor targeting through gold particle drug delivery.⁵ This method involves precipitation of Iron (II) and Iron (III) oxide nanoparticles from increasing the pH of an acidic solution containing dissolved iron ions. The pH, salt concentration, and ionic strength all affected the size of the nanoparticle produced.⁵ Following the precipitation of iron oxide, there were two major products present, magnetite and maghemite. Maghemite (Fe_2O_3) has been shown to have a higher affinity for gold association than magnetite (Fe_3O_4).¹⁵ To drive the iron oxide particles to preferentially form maghemite, nitric acid was used in excess as an oxidizing agent. To prevent aggregation, tetramethylammonium hydroxide was added. The gold coating was formed by adding chloroauric acid while heating the solution; the specific temperature was not mentioned.

Multiple particle types were synthesized by the Wagstaff group, including untreated iron nanoparticles, Fe@Au nanoparticles, Fe@Au nanoparticles conjugated with polyethylene glycol (PEG), and PEGylated Fe@Au nanoparticles functionalized with cisplatin. The Ultraviolet-Visible (UV-Vis) spectrum obtained contained absorption patterns for all four nanoparticle types, but only patterns for the gold-coated iron and uncoated iron showed absorbance in the visible range. The most notable differences in absorption were that the gold coated iron particles had a slight absorbance at a wavelength similar to that which colloidal gold absorbs, at approximately 560 nanometers (nm). The untreated iron nanoparticles absorb wavelengths below 450 nm. The TEM images showed that the gold-coated iron particles had obvious variation in particle size and gold shell thickness produced by this method.

The resulting magnetic properties of the co-precipitation synthesized nanoparticles made by Wagstaff *et al.* were not characterized via traditional means, but were observed visually by resting a magnet near a flask containing the nanoparticles in solution. The key concern for this group was the cytotoxicity of the cisplatin functionalized nanoparticle variants to cancerous ovarian cells. The gold shells formed by this method were large, but nanoparticle size distribution wasn't narrow enough for biosensor applications.

Micellar-Based Reduction

One group that investigated the use of an inverse micelle for Fe@Au nanoparticle synthesis was Lin *et al.*⁶ By controlling the ratio of water to surfactant, the size of the inverse micelle and the nanoparticle size can be also be controlled.⁶ The surfactant and

co-surfactant used were cetyltrimethylammonium bromide (CTAB) and 1-butanol, respectively. The source of iron was iron sulfate heptahydrate, and the source of gold was chloroauric acid. The reducing agent used to precipitate solid iron was sodium borohydride. Mixing of the chemical reagents was done under nitrogen to prevent oxidation of uncoated iron nanoparticles.⁶

The product was characterized by Scanning Electron Microscopy (SEM), UV-Vis spectroscopy, powder X-Ray Diffraction (XRD), and DLS. The size distribution of the nanoparticles, from dynamic light scattering analysis, ranged from 30 to 80 nanometers.⁶ The Lin group noted that this was most likely due to agglomeration of the product, which was confirmed to be much more common for gold-coated nanoparticles than pure colloidal gold.⁶ TEM imaging was in good agreement with results from DLS. Particle size was smaller than the average value given by DLS measurements, according to TEM images.

Lin *et al.* used ZFC and FC magnetization as a method for studying their particle's blocking temperature. According to their results, at 42 K the maximum magnetization level is observed. At higher temperatures the particles are superparamagnetic and magnetize reversibly. The apparent blocking temperature of 42 K implies that below this temperature, the magnetic properties of the particles are irreversible and the particles act ferromagnetically. The group performed hysteresis characterization at varying temperature ranges and confirmed that at high temperatures (300 K) no magnetic coercivity was observed for the nanoparticles. Below 42 K (10 K and 2 K) a respective coercivity of 728 Oe and 322 Oe were observed.

Fe@Au particles formed using this method have a size dependence on reagent ratios, which can be manipulated, and are easily formed at room temperature in a short time period.

“TOP-DOWN” SYNTHESIS METHODS

Electroless Gold Plating onto Nanobeads

An electroless gold plating method was described by Zhang *et al.*, that reacted commercially purchased magnetic polystyrene nanobeads with stannous chloride, then deposited a small silver layer through redox interaction onto the surface of the polystyrene.⁷ The silver layer acted as a catalytic site for gold seed formation of sodium gold sulfite. The product developed from this synthesis method was used for immunoassay applications, to test antibody binding efficiency and analytical properties.⁷ The magnetic Dynabeads® provided a level of uniformity necessary for their project’s stipulations.

The layer of gold on the surface, which was approximately 6 to 7 nm thick, was not visible relative to the large nature of the purchased polystyrene beads, which were 450 nm in diameter. The verification of the gold layer coating was provided through X-ray Photoelectron Spectroscopy (XPS) measurements. The additional nanoparticles evaluated in their XPS spectrum were tin-coated and silver-coated polystyrene beads. No magnetic saturation characterization was performed. Based on the relative size of the various coatings compared to the magnetic nanobeads, the group postulated that there would be a negligible loss of magnetic properties resulting from the coating process.⁷ They visually observed no apparent difference in reaction of the beads to a magnetic

field, whether coated or uncoated.⁷ They also compared settling times for the coated and uncoated beads. The beads that were coated with gold did settle 1.22 times faster than uncoated beads, likely due to the increase in particle density.⁷

The particles used for this experiment were too large to be effectively mobile in a biosensor platform.

Reduction of Gold onto Iron Nanospheres and Nanorods

Chen *et al.* performed gold-coating deposition on both commercially obtained iron nanorods and synthesized spherical iron nanoparticles.⁸ The method for spherical iron nanoparticle formation involved the thermal decomposition of iron pentacarbonyl in dioctyl ether using cobalt acetylacetonate as the catalyst for reduction and capping agent. The creation of the gold layer on the iron surface for the rods and spheres was performed using mild reducing agents and gold acetate. The TEM images showed that the iron rods were significantly larger than the synthesized iron spheres (200 nm length rods versus 12 nm diameter spheres). The distribution range of the coated iron nanospheres was large, with particles as small as 2 or 3 nanometers, and as large as 25 nanometers. The large iron rods were coated with gold clusters instead of a well-defined gold layer.⁸ The reduction process used was not clearly described, but was initiated using a “mild reducing agent”, from an organic gold source. It is possible that, similar to the Robinson group, using an organic gold source has decreased the effectiveness of gold seeding at the particle-solvent interface.

The magnetic properties of the Chen product were measured while varying temperature and pH. They purchased iron nanorods for the gold coating process. They

didn't compare results of magnetic properties for both coated and uncoated iron nanospheres. The group measured the magnetization of the particles, and determined that the large coercivity values for the acicular iron rods are attributed to the native oxide layer present in the structures.⁸ The acid effect seems to show that as more of the iron is oxidized, the lower the magnetic saturation value becomes. This is logical since iron oxide has a smaller magnetic moment than elemental iron.⁸

The gold shell formed using this approach wasn't thick enough to prevent iron core oxidation, and the procedures required the use of toxic and air-sensitive chemicals (iron pentacarbonyl).

Magnetization of Superatomic Gold Clusters

Another approach to forming gold particles susceptible to magnetic field control was developed recently by McCoy *et al.*⁹ By introducing a strong oxidizing agent to special "superatom" gold clusters, the removal of an electron causes the electronically closed-shell compound to become paramagnetic. Chloroauric acid was dissolved in nanopure water, and mixed with a basic solution containing *p*-mercaptobenzoic acid and methanol. Sodium borohydride was added to reduce gold (III) to metallic gold. This resulted in the formation of the "superatom" gold clusters, having the structure $A_{102}(p\text{-MBA})_{44}$. The solid product is dissolved in a basic borate buffer and oxidized with potassium permanganate. The product was washed quickly, since over-exposure to a strong oxidizing agent can also cause the cluster size of the superatom to increase.

Superatom gold clusters made by the McCoy group were not characterized using microscopy. The approach used by this group to determine success of the synthesis was

done via proton Nuclear Magnetic Resonance (^1H NMR). The gold clusters which were oxidized showed a splitting pattern in the solvent peak in the ^1H NMR analysis. The control sample of unoxidized gold clusters did not.¹⁶

The effect of the magnetic field (produced by a RF signal of 13.56 MHz) on the gold superatoms caused an increase in temperature of the surrounding system of almost 5 degrees Celsius ($^{\circ}\text{C}$). The intent of their publication was to determine the ability of these gold clusters to respond to a RF signal in a similar way that super paramagnetic iron oxide particles respond to an oscillating magnetic field.

Since the method for producing the superatomic gold clusters was complex and involved expensive chemical reagents, it was not chosen as the preferred synthesis method for magnetic gold nanoparticle production.

ASSIGNING THE PREFERRED SYNTHESIS METHOD

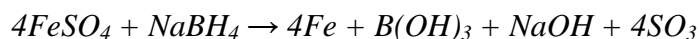
There are several factors to consider when selecting the ideal approach for nanostructure formation. They are dictated by any intended purposes for the product. Particle size distribution, uniformity, reproducibility and chemical consumption costs are extremely important factors with regards to synthesizing nanoparticles intended for clinical use.² Consistency in performance and analysis results are paramount in medicinal applications. Comparing the resulting gold-coated magnetic particles of these different groups provides insight relative to reproducibility, particle uniformity, and magnetization effects.

The Lin method appears to be the most appealing method in terms of nanoparticle size control. The Robinson method appeared to have narrower particle size distribution.⁴

Coating commercially available magnetic beads with gold will lead to products with excellent magnetic properties. Beads of this size often cannot be used for biomedical applications. When choosing the correct method for any potential nanoparticle synthesis, the major factor to consider is which desired nanoparticle properties are of highest priority. The assigned method chosen was the micellar-based reduction, or the Lin method.

The Lin method to nanoparticle synthesis consists of three key steps: formation of the inverse micelle, formation of the iron nanoparticles, and nucleation and propagation of the gold atoms at the particle surface. The initial step involves mixing CTAB and aqueous iron sulfate together in octane and butanol. This forms the inverse micelle, whose size is directly proportional to the ratio of water to surfactant (H₂O/CTAB). The ratio used by Lin *et al.* was 8.

For the step involving formation of the iron nanoparticles, a strong reducing agent contained within an inverse micelle solution (of similar size) was introduced to the solution. The proposed reaction mechanism is shown below:



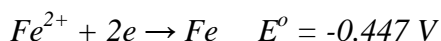
The sodium borohydride donates 8 electrons to form boron trihydride in the presence of oxygen. These electrons can reduce iron in the ferrous sulfate molecules from its Iron (II) oxidative state down to Iron (0), forming elemental iron nanoparticles.

The gold layer is then formed at the surface of the iron nanoparticles by adding chloroauric acid contained within an inverse micelle solution in the presence of excess sodium borohydride. The proposed reaction mechanism is shown below.

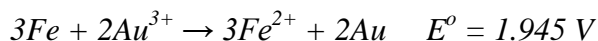


OPTIMIZING THE PREFERRED SYNTHESIS METHOD

Improving nanoparticle quality to a level expected for an application requires the modification of the Lin synthesis method to increase synthesis efficacy and reproducibility. The magnetic properties of the nanoparticles can be directly influenced via the inverse micelle to control the size of the nanoparticle. The reduction of the gold in the chloroauric acid to elemental gold in the third step of the process could be removed because of iron's inherent reduction potential illustrated by its ΔE value listed in the electrochemical series. The preferred reduction at the iron nanoparticle surface would also minimize the formation of gold colloid. The reduction potential reactions are shown below:



The stoichiometry of the reduction reaction between iron and gold atoms proposed and the resulting potential is shown below:



The calculated Gibbs free energy from the reaction is 1126 kJ/mol. The redox reaction between the iron nanoparticle surface and aqueous trivalent gold atoms is spontaneous.

In aqueous solutions, gold nanoparticles are surrounded by an electrical double-layer (EDL) composed of ions.¹⁷ The size of the layer dictates a particle's stability and likelihood to aggregate, due to the electrostatic repulsive force created from interaction of two adjacent and similarly-charged EDL's. If a particle's EDL doesn't have a high enough potential, it is likely to aggregate and fall out of suspension. A monodisperse solution is needed for biosensor applications, so aggregation was avoided by functionalizing the particle surfaces with carboxy thiol polyethylene glycol (CT-Peg). Sulfur binds to the gold surface, and the polyethylene glycol chain acts as a spacer to prevent aggregation.

Evaluation of inverse micelle size was performed by using dynamic light scattering measurements to study the solutions with variable water to surfactant ratios. The relationship between reagent ratio and micelle size was then established. To effectively determine the reliability of the measurements, a nanoparticle control sample was used and the deviation of the measurements calculated. The sizes 8 molar ratio Fe@Au particles and 20 molar ratio Fe@Au particles were analyzed. As a control, 20 molar ratio uncoated iron nanoparticles (iron oxide) were also studied.

The efficacy of the iron reduction potential was studied by colorimetric comparison. Due to the inert conditions under which the reaction proceeds, the color of the solution indicated if any oxidation of iron and reduction of gold was occurring.

Modifying the synthesis method in the fashion previously mentioned should result in two major benefits. By optimizing the magnetic properties of the nanoparticles, the efficiency of the biosensor method will be vastly improved. Through manipulating the micelle ratio, the size of the particles to be used in the biosensor can be controlled. By inducing gold atom nucleation without the use of additional reducing agent, zero-valent gold formation should be localized at the nanoparticle surface as opposed to spontaneous gold atom nucleation in solution. This will reduce the cost of the synthesis method. Less reducing agent and chloroauric acid would be needed to create the same product.

CHAPTER III

EXPERIMENTAL METHODS

The following reagents were purchased from Fisher Scientific and used as received: iron sulfate heptahydrate ($\text{FeSO}_4 \cdot 7\text{H}_2\text{O}$) [Product # 423731000], CTAB ($(\text{C}_{16}\text{H}_{33})\text{N}(\text{CH}_3)_3\text{Br}$) [Product # 0219502990], 1-butanol ($\text{C}_4\text{H}_9\text{OH}$) [Product # A399-500], n-octane (C_8H_{18}) [Product #325950025], chloroauric acid trihydrate ($\text{HAuCl}_4 \cdot 3\text{H}_2\text{O}$) [Product # 411070050], and 12% (w/w) sodium borohydride (NaBH_4) in 40% sodium hydroxide (NaOH) [Product # 389930010]. All water used was ultrapure 18 millipore water.

Preparation of Micellar Solutions

Six grams of CTAB, 5 grams of 1-butanol, and 15 grams of octane were combined in a beaker and stirred using a magnetic stir plate for 15 minutes. An aqueous iron sulfate solution of 0.5 M concentration was then added to the surfactant mixture, creating an inverse micelle. The volumes of iron sulfate solution used were 2.4 mL, 3.57 mL, 4.75 mL, 5.83 mL, 6.99 mL, and 8.16 mL to create separate 8, 12, 16, 20, 24, and 28 molar ratio solutions respectively. The solutions were allowed to continue stirring for 10 minutes or until the solution became homogenous and acquired a light aquamarine coloration. Three solutions of each molar ratio were made. Five mL of each solution was taken and diluted in a 1:1 ratio with n-octane over a magnetic stir plate for 15 minutes. These aliquots were used for inverse micelle size measurements via DLS. The 8 and 20 molar ratio solutions were transferred to a 250 mL round bottom flask for degassing and mixing under an inert blanket of argon for one hour.

The reducing agent was prepared via a similar process, by mixing the same masses of CTAB, 1-butanol and n-octane in a similar fashion as described previously. Sodium borohydride solutions with volumes of 2.4 mL or 5.65 mL and a concentration of 1.0 M were then added to their respective mixtures forming inverse micelles of 8 and 20 molar ratio water to CTAB, respectively. The concentration of the reducing agent added in the previous step was adjusted to 0.125 M for the experiment designed to test the reduction potential of the iron nanoparticles *in situ*. The micellar solution was stirred for 10 minutes until the solution became homogenous and translucent. In order to maintain an inert environment in the reaction flask, this solution was injected into the flask using a 60 mL syringe through a septum in a drop wise fashion, creating a black solution. The Iron (II) from the iron sulfate solution was allowed to reduce in the reaction flask for a period of thirty minutes while being stirred. One solution containing 20 molar ratio reduced iron nanoparticles was removed from the flask at this point and allowed to oxidize, to be used as a control sample for nanoparticle property comparison between Fe@Au particles and uncoated iron particles.

The chloroauric acid solution was prepared by mixing 3 grams of CTAB, 2.5 grams of 1-butanol, and 10 grams of octane and stirring using a magnetic stir plate. Aqueous chloroauric acid solutions of volume 1.8 mL or 4.24 mL and a concentration of 0.44 M were then added to their respective mixtures and allowed to stir for 10 minutes or until the solution became homogenous and had a burnt orange appearance. This mixture was then added to the reaction flask through the septum in a similar fashion to that described above. The resulting color of the solution at this point was dependent on

concentration and volume of reducing agent used. The nanoparticle solutions were allowed to stir for a minimum period of one hour.

The iron nanoparticle solutions were transferred to a 250 mL beaker and placed in the magnetic field of Cahn-Ventron 5700 gauss magnet for twelve hours in order to separate the magnetic nanoparticles from the supernatant liquid. The supernatant liquid was then either decanted or removed using a pipette. The remaining nanoparticle products were washed with methanol (CH_3OH) and chloroform (CHCl_3), in a 1:1 ratio and isolated by centrifugation at 10,000 rpm for 15 minutes. This magnetic pull-down and wash process was repeated twice. The nanoparticles were washed with H_2O and centrifuged at 15,000 rpm for 15 minutes a total of three times.

Functionalization of the Nanoparticle Surface

The stability of the nanoparticles in solution was improved by treating the gold nanoparticle surface with CT-Peg [Product # 26133]. A phosphate buffer solution of volume 150 mL and a pH of 7.4 was made using 20 mM sodium phosphate dibasic (Na_2HPO_4) [Product # BP331-500] and 20 mM sodium phosphate monobasic (NaH_2PO_4) [Product # S381-500], in 0.1 M aqueous NaCl. One hundred mL of this buffer was used as a solvent for the reaction between the sulfur head group of the CT-Peg molecules and the gold on the nanoparticle surface. Nanoparticle aggregation was minimized before functionalization using ultrasound sonication with cycles of 15 seconds on, 2 minutes off for 6 minutes at an amplitude of 25% using a probe-tip sonicator. In a separate beaker, 5 mL of a solution containing 4 mM CT-Peg in 40 mL of dry dimethylformamide was added to the remaining 50 mL of the PBS solution and stirred for 10 minutes using a

magnetic stir plate. This CT-Peg solution was added in 10 mL/min increments to the nanoparticle/PBS mixture with magnetic stirring, and then incubated at 22°C for two hours. The nanoparticles were removed using centrifugation and washed with H₂O to remove excess CT-Peg.

Ion Exchange Treatment

The removal of any residual surfactant (CTAB) in the nanoparticle solution was attempted using cationic exchange treatment. The stationary phase utilized was Purolite® LT100 Resin Beads. A flash-chromatography column was used of size 38 mm x 560 mm. The resin was positively charged using a 1.0 M NaCl solution for 15 minutes. The mobile phase employed for nanoparticle transport through the column was a 10 mM NaCl solution, which was followed with a 100 mM NaCl solution wash of the column for removal of the adsorbed CTAB. The nanoparticles were run through the column 3 times and then centrifuged and resuspended in ultrapure H₂O.

Light Scattering Measurements

A Malvern dynamic light scattering Zetasizer Nano was used to perform all light scattering measurements described. The defined parameters for the micelle size determination trials were as follows: refractive index of gold in water = 1.59, refractive index of water = 1.33, quartz cuvette of length 1 centimeter, room temperature = 22 °C. All gold nanoparticle measurements were taken after 2 minutes of stabilization. Inverse micelle measurements were not stabilized prior to measurements. Iron oxide measurement parameters are the same as above except the refractive index for the analyte

was 2.42. The parameters for the inverse micelle measurements were as follows:
refractive index of analyte (water) = 1.33, refractive index of solvent (octane) = 1.398
with a viscosity of 0.51 cP.

SEM Analysis

Samples of the nanoparticles were typically prepared for scanning electron microscope analysis by spin-coating 0.5 – 2.0 mL of a 1% by weight nanoparticle solution onto a small silicon wafer, or by dropping one drop of the nanoparticle solution on toluene and allowing it to air dry. The wafer was stored for at least 24 hours in a vacuum oven at approximately 70°C at a pressure less than 5 torr. The scanning electron microscope used was manufactured by FEI, the model was a Helios Nano Lab 400. SEM samples were also analyzed using TEAMTM software designed by EDAX © to perform electron dispersive x-ray spectroscopy which gives elemental identification of the sample.

UV-Vis Spectroscopy

All samples that were analyzed using ultraviolet-visible spectroscopy were analyzed using a Varian Cary 100 spectrophotometer. The wavelengths analyzed were from the 200 to 800 cm^{-1} signal range, with zero and baseline corrections against nanopure water. The cuvettes used were made of quartz, and were the standard length and width of 1 cm. To prepare solutions for UV-Vis analysis, 1-3 mL of each nanoparticle solution were diluted in 100 mL of water and mixed via ultra-sonication with cycles of 10 seconds on, 50 seconds off for 3 minutes at an amplitude of 25% power.

Magnetic Hysteresis Characterization

To examine hysteresis loop patterns of the nanoparticle products, a vibrating sample magnetometer was used. Changes in magnetic moment were measured while varying the applied magnetic field from -60 kOe to 60 kOe, at temperatures of 10, 100, and 300 K.

TGA Trials

Powder samples of the varying nanoparticle products were made by transferring 10 mL of the desired solution to a 20 mm watchglass, and drying the sample under vacuum for 24-48 hours. A metal spatula was used to collect the dried powder. The instrument used for analysis was made by TA instruments, model Q50. The program specifications for each trial consisted of a temperature ramp from room temperature (22 °C) to 800 °C at a rate of 20 °C/min while recording sample mass change.

CHAPTER IV

RESULTS AND DISCUSSION

EVALUATION OF DIFFERENT MICELLE SIZES

Dynamic Light Scattering

Light scattering results from a trial analyzing the 20 molar ratio water to CTAB solution are shown below in Figure 2. The micelle size for this sample was 58.74 nanometers. The shape of the micelle size distribution is narrow and sharp. A second micelle was also observed with a size slightly greater than 600 nanometers.

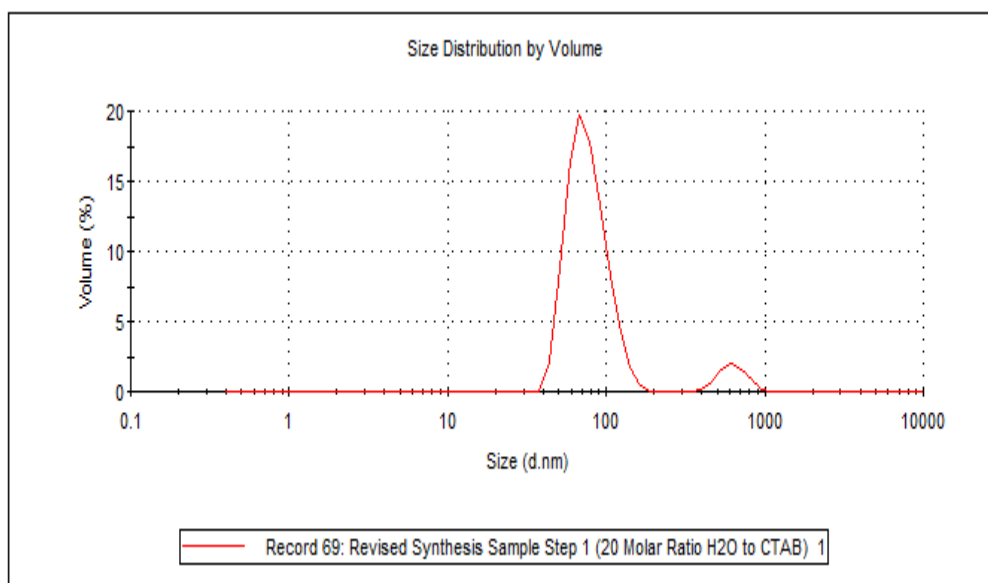


Figure 2: DLS Data for 20 Molar Ratio Inverse Micelle. Dynamic light scattering size distribution by volume of the micelle created using a 20 molar ratio of water to CTAB.

The inverse micelle size determination trials showed a direct relationship between micelle diameter and phase ratio solutions containing between 8-20 molar ratio of water to CTAB and produced a trend line with an r-squared value of 0.975 (Figure 3).

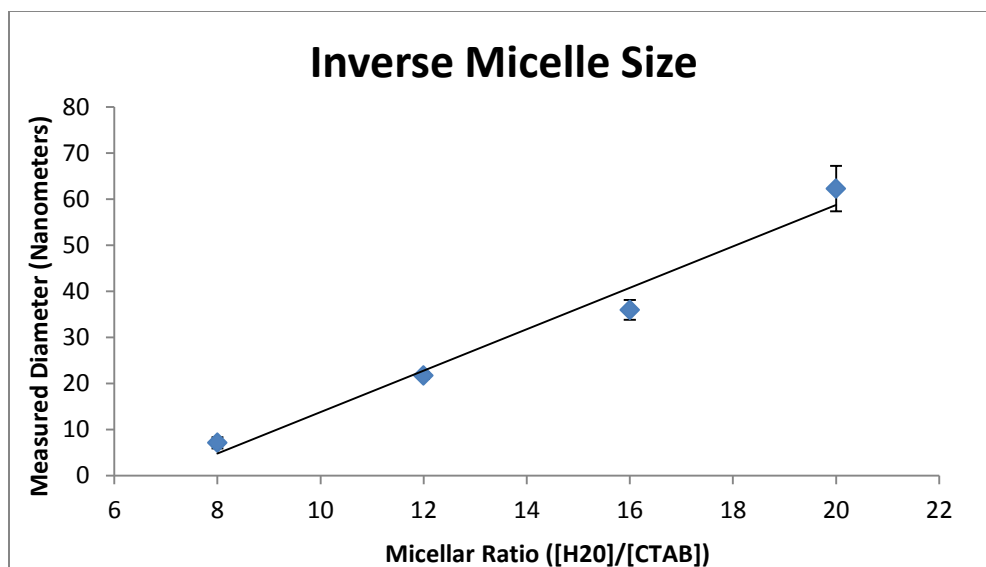


Figure 3: Inverse Micelle Sizes. Light scattering values for the micelle size versus micellar ratio (linear range).

Solutions with a 24 and 28 molar ratio of water to surfactant were unstable. As such, after a brief period the micelle disassociates and forms a more stable complex, averaging around 10 to 30 nanometers, depending on the phase ratio. This indicates that the critical surfactant concentration exists near the water to CTAB molar ratio of 20.

NANOPARTICLE PRODUCT CHARACTERIZATION

Dynamic Light Scattering

Colloidal gold products were obtained from Sigma Aldrich and were used to determine the accuracy of measurements made by the Malvern Dynamic Light Scattering instrument. Particle sizes used for the tests were 5, 10, 20, 40, 100, and 200 nm. The majority of the analyses yielded readings with high accuracy and precision (Figure 4). The largest discrepancy between actual particle size and analysis results was found for the 100 nm particle solution, where the Malvern calculated a size of approximately 120

nm. The trend line shown in the graph had an r-squared value of 0.993. The linear equation for the trend line was $y = 0.9515x + 12.184$, which was calculated to use as a correction factor for the light scattering results from actual Fe@Au particle size measurements.

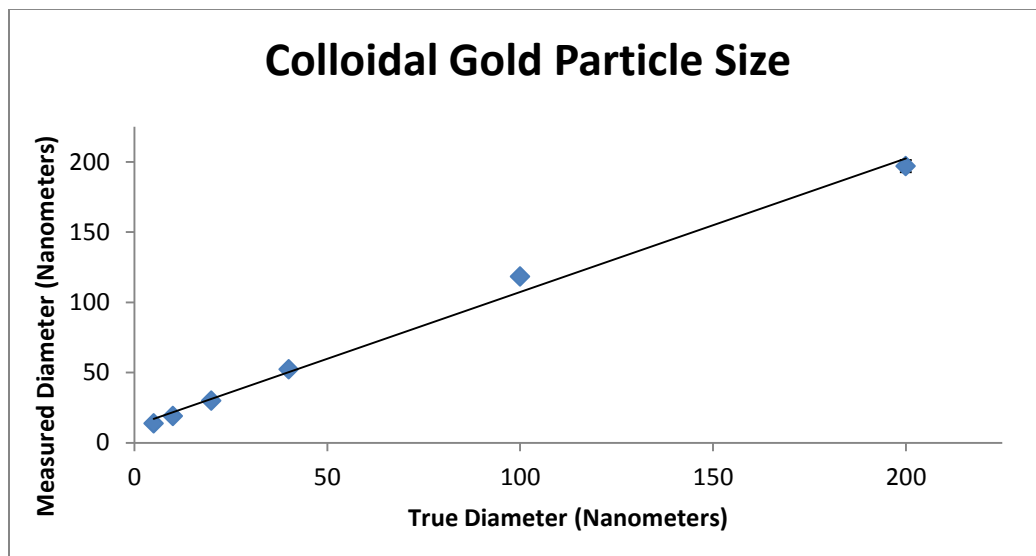


Figure 4: Colloidal Gold Particle Sizes. Light scattering values of the commercially purchased colloidal gold's measured diameter versus true diameter values.

Size distribution analysis for one of the 20 molar ratio gold-coated iron nanoparticles measurements is shown below in Figure 5. A much wider distribution curve was observed compared to the curves obtained from micelle size analysis.

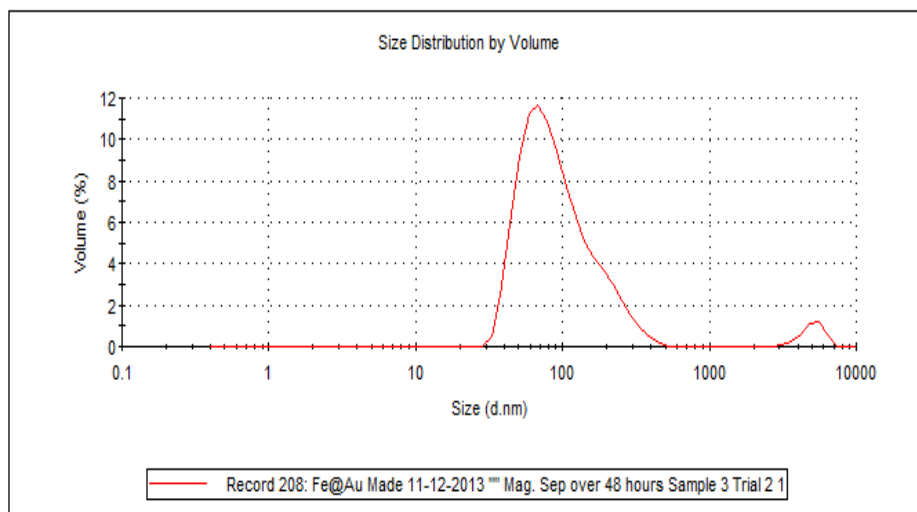


Figure 5: DLS of 20 Molar Ratio Fe@Au Product. Size distribution analysis of one sample of the Fe@Au particles synthesized.

The Fe@Au particles had an average size of 126.58 nanometers, with a standard deviation of 5.53 nanometers and a standard error of 1.84 nanometers. Using the correction factor from the gold colloid analysis, the true particle size was calculated to be 120.23 nanometers. Iron oxide nanoparticles from the same ratio had an average size of 217.56 nanometers, with a standard deviation of 16.01 nanometers, and a standard error of 9.25 nanometers. The correction factor could not be applied to the iron oxide nanoparticles, because an iron nanoparticle control sample was not available to first establish the accuracy of light scattering iron particle measurements. Gold-coated iron had significantly lower standard deviation and standard error values than iron oxide, and was therefore more consistent. The stabilizing agent used, CT-Peg, was only used on the gold-coated iron, and is the reason for a decrease in aggregation in solution for the gold-coated particles versus the iron oxide.

A monodisperse nanoparticle product was not obtained, and it is possible that the CT-Peg stabilization wasn't completely effective. CT-Peg functionalization wasn't

performed until after the purification of the nanoparticle product, so particle aggregation was occurring prior to functionalization.

SEM Analysis

Scanning electron microscope images of the 8 molar ratio Fe@Au product are shown below in Figure 6. The particles are approximately 5-15 nanometers in diameter, and according to energy dispersive X-ray spectroscopy analysis are approximately 13% gold and 41% iron with peaks at 2.12 eV and 0.67 eV respectively (Figure 7). These percentages are calculated by relative photon counts calculated by the software. Silicon and oxygen signals peaks at 1.9 eV and 0.6 eV in the Energy Dispersive X-Ray Spectroscopy (EDS) spectrum are attributed to the substrate used for sample placement,

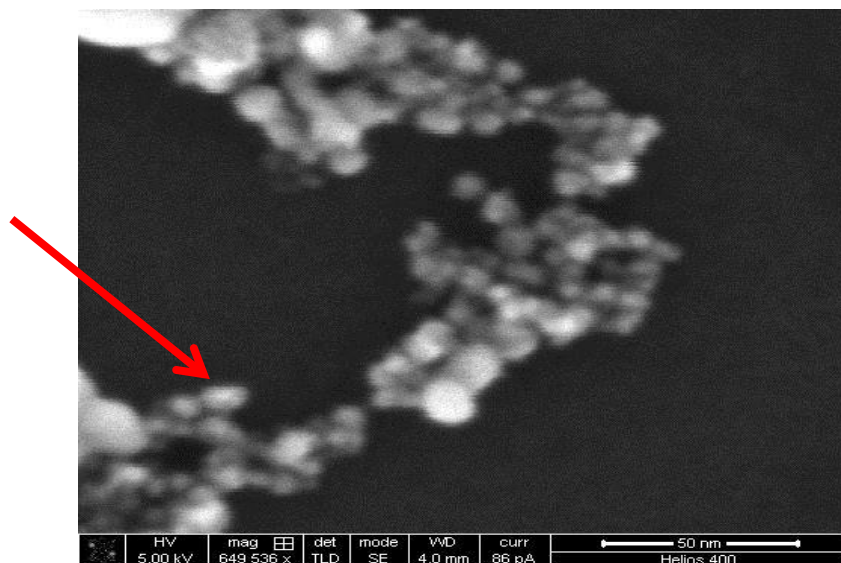


Figure 6: SEM Image of 8 Molar Ratio Fe@Au Product. A scanning electron microscope image of the Fe@Au product using the 8 molar ratio. The arrow shows a particle that is spherical.

composed of silicon with an oxide surface layer. The majority of the particles are near spherical. There appears to be some aspherical particles as well (Figure 6, red arrow)

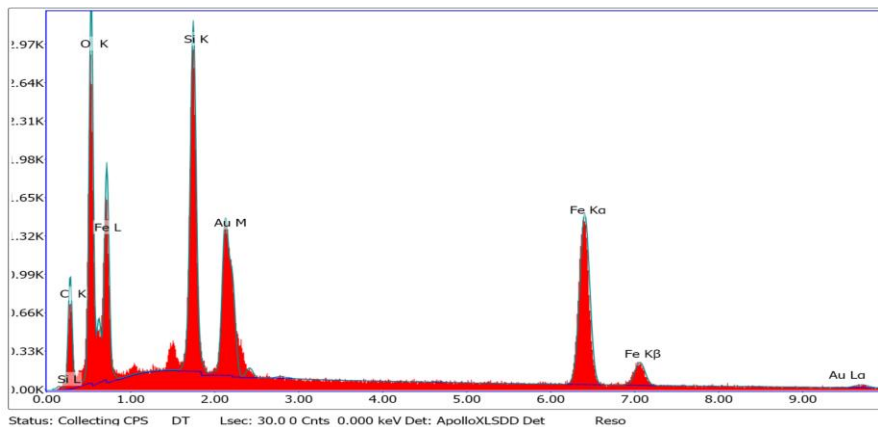


Figure 7: EDS Spectrum of 8 Molar Ratio Fe@Au Product. An electron dispersive X-ray spectrum from a sample of Fe@Au nanoparticles synthesized via the Lin method. The x-axis has units of eV, and the y-axis has units of count number (intensity).

The images of the 20 molar ratio Fe@Au nanoparticle product in Figure 8 are significantly larger than the 8 molar ratio product, with an average diameter of 73 nanometers and a size range of 55-95 nanometers. EDS analysis confirmed the presence of both gold and iron in the product (in addition to the X-rays produced by the substrate), at a percent composition of 44% and 10% with peaks at 2.12 eV and 0.67 eV, respectively (Figure 9). The SEM images showed that particle size is smaller than the values calculated by DLS, it is likely that aggregation in solution is responsible for this discrepancy.

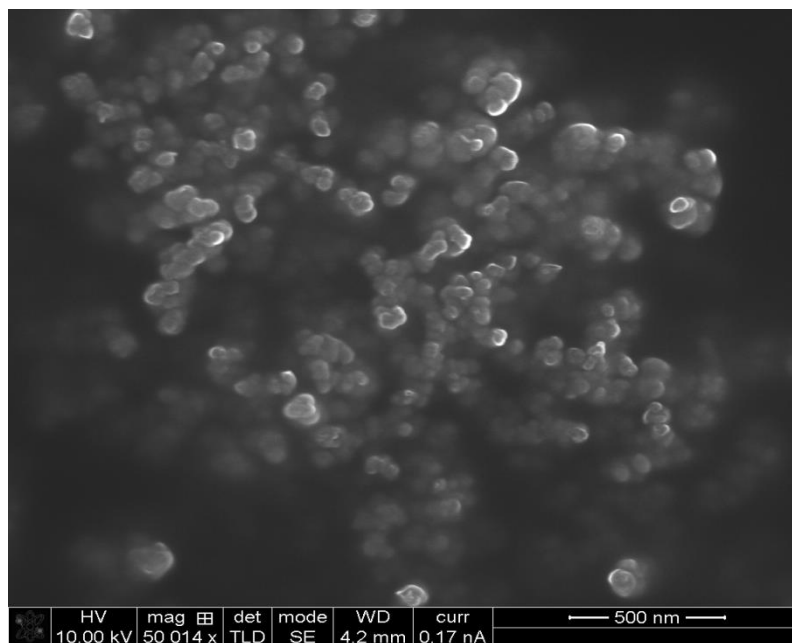


Figure 8: SEM Image of 20 Molar Ratio Fe@Au Product. A scanning electron microscope image of clusters of the 20 molar ratio Fe@Au nanoparticle products.

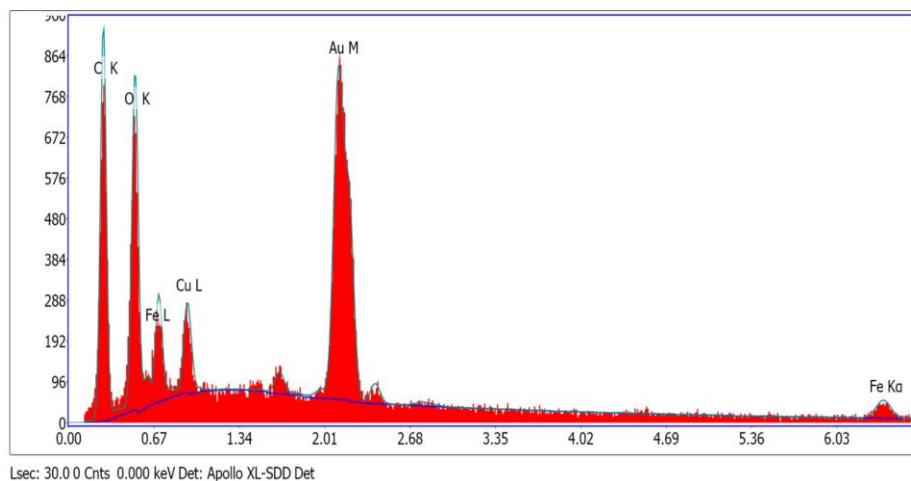


Figure 9: EDS of 20 Molar Ratio Fe@Au Product. An electron dispersive X-ray spectrum from a sample of the 20 molar ratio gold coated iron products. The x-axis has units of eV, and the y-axis has units of count number (intensity).

SEM images of the iron oxide nanoparticles made using a water to CTAB molar ratio of 20 can be seen below in Figure 10. The particle sizes range from 20 nanometers to 50 nanometers. The particle shape is primarily spherical with some needle shaped iron

particles. Elemental analysis showed a large oxygen peak and a small iron peak (Figure 11). The substrate peak, silicon, accounts for 54% of the signal, oxygen accounts for 37%, and iron accounts for 9%. The silicon/oxygen ratio was larger than on the substrate-only EDS analysis (Figure 12). Since the particles are iron oxide, a decrease in the ratio would be expected. EDS analysis is excellent for identifying composition; the results are not always quantitatively accurate. To improve the EDS analysis results in the future, the intensity of the electron beam can be adjusted to decrease X-ray penetration of the sample. This would produce more accurate elemental characterization of particles on the surface of the substrate. When looking at samples at high magnification, other problems such as sample drift can become a major cause of inconsistency in EDS measurements.

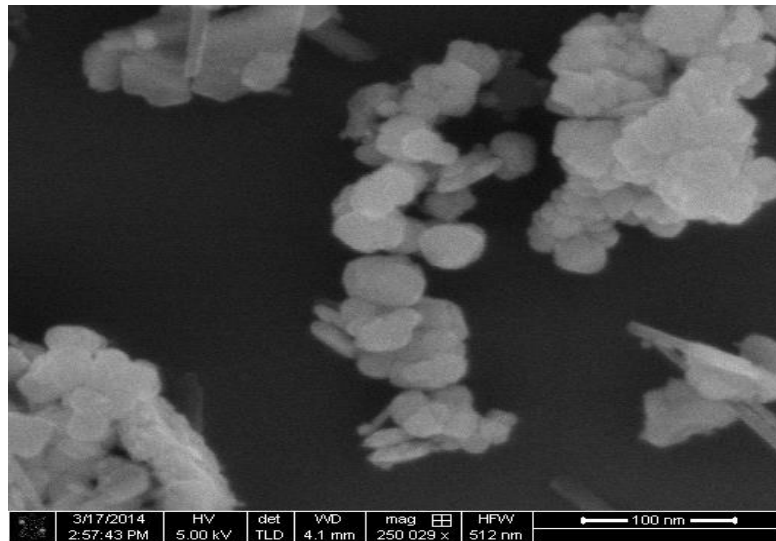


Figure 10: SEM Image of 20 Molar Ratio Iron Oxide Product. A scanning electron microscope image of iron oxide nanoparticles produced using the 20 molar ratio.

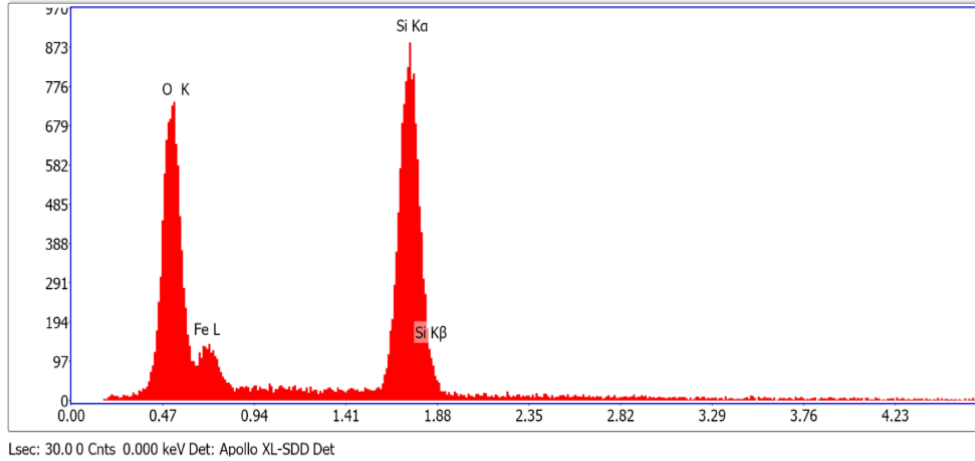


Figure 11: EDS of 20 Molar Ratio Iron Oxide Product. An electron dispersive X-ray spectrum from a sample of the iron oxide nanoparticles. The x-axis has units of eV, and the y-axis has units of count number (intensity).

An elemental analysis was performed on the substrate used for the iron oxide product as a control, and the results are shown in Figure 12. This was performed because the ratio of oxygen to iron needed to be determined, and the substrate had a native oxide layer. The substrate surface was determined to be 57% silicon and 43 % oxygen with peaks at 1.75 eV and 0.49 eV respectively.

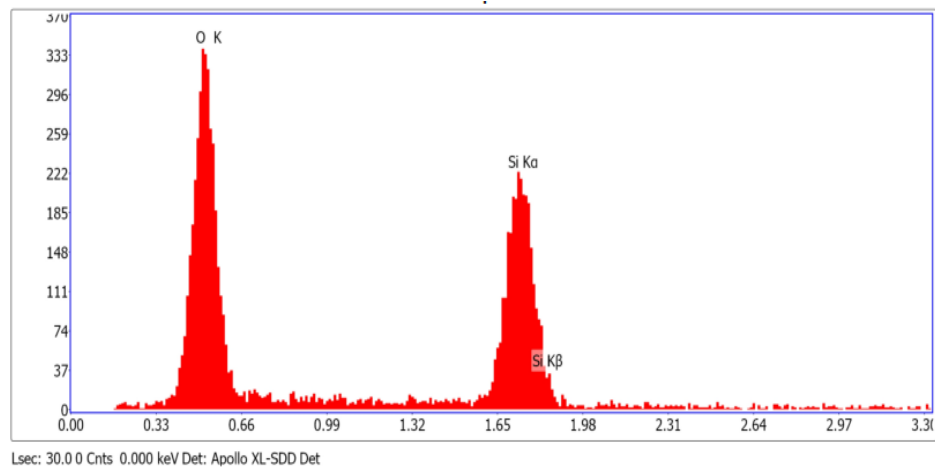


Figure 12: EDS of Silicon Oxide Substrate. An electron dispersive X-ray spectrum from the sample substrate, a silicon wafer coated with silicon oxide. The x-axis has units of eV, and the y-axis has units of count number (intensity).

UV-Vis Absorbance

The surface plasmon of metallic particles is affected by particle features such as shape geometry, dimension, and aggregation in solution.¹⁸ The peaks of visible and ultraviolet light absorbance by each solution are indicative of not only the composition of the particles present, but also the particle characteristics. The absorption patterns of 100 nm colloidal gold nanoparticles and a 1% solution of the supernatant obtained post particle functionalization and centrifugation have a high degree of similarity (Figure 13). The peak absorption occurs at 525 cm^{-1} for colloidal gold (represented by the red line), and 530 cm^{-1} for the supernatant solution (represented by the blue line) in Figure 13. The supernatant UV-Vis absorbance spectrum implies that colloidal gold was formed in the reaction solution. Excess reducing agent in the inverse micelle was likely to have caused spontaneous gold colloid formation, explaining this absorbance pattern for the supernatant. The increase in peak width for the supernatant solution isn't surprising since the size distribution and particle aggregation are larger than the commercially purchased colloidal gold solution.

The absorption spectra of iron oxide nanoparticles and gold coated iron nanoparticles are shown below in Figure 14. The purple line represents the Fe@Au nanoparticles while the red line represents the iron oxide nanoparticles. Both particle types exhibit absorption below 500 nanometers but the Fe@Au NP's exhibit additional absorption at 530 nm. This is indicative of the presence of gold in the particles since strong absorption in this area is attributed to gold's visible light patterns.

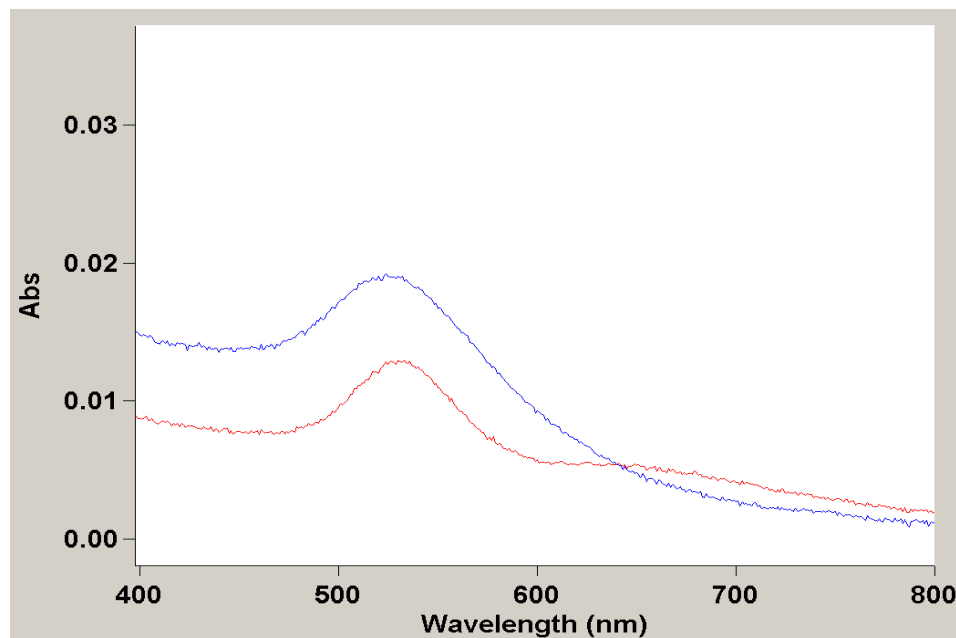


Figure 13: UV-Vis of Supernatant versus Gold Colloid. UV-Vis spectrum of commercially purchased colloidal gold particles (red line) and the supernatant obtained after centrifugation of CT-Pegylated gold-coated iron (blue line).

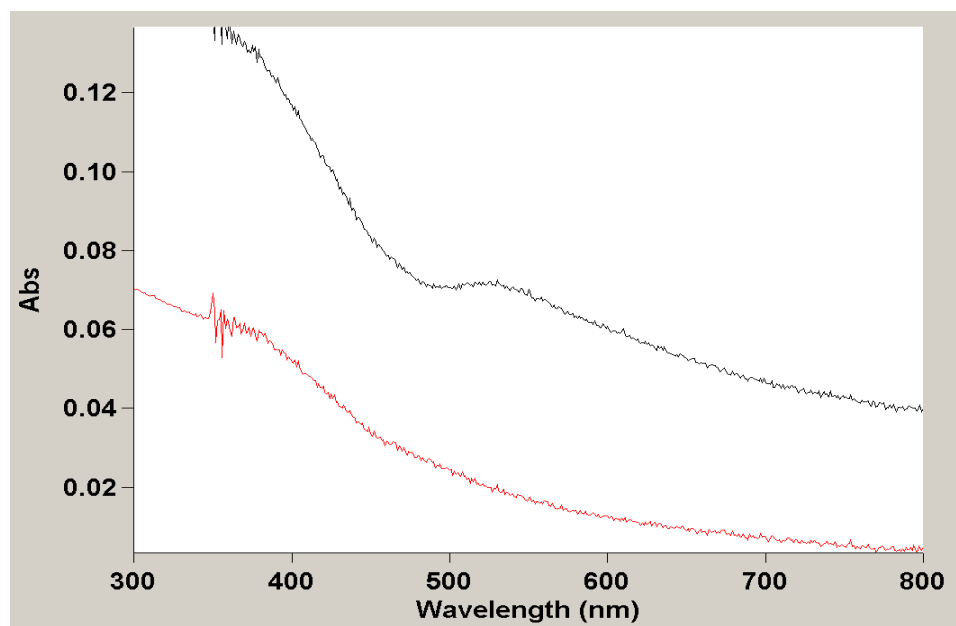


Figure 14: UV-Vis of Fe@Au versus Iron Oxide Product. UV-Vis spectra of the iron oxide nanoparticle product (red line) and the gold-coated iron nanoparticle product (black line).

Magnetic Hysteresis Characterization

The magnetic properties of the Fe@Au and uncoated iron 20 molar ratio nanoparticle products were evaluated using VSM instrumentation to test hysteresis patterns by measuring magnetic moment with respect to applied magnetic field. Values determined include magnetic saturation, magnetic coercivity, and magnetic remanence. Figure 15 is the hysteresis loop for the iron oxide product, at 10 K. The magnetic saturation is $1.16 \times 10^{-5} \text{ Am}^2$, magnetic coercivity is -450 and +380 Oe, and remanence was $4.44 \times 10^{-6} \text{ Am}^2$. The coercivity value isn't surprising since the iron oxide formed contains maghemite and magnetite. The latter has strong magnetization potential. Figure 16 is the hysteresis loop for the Fe@Au particles, at 10 K. This product showed a magnetic saturation of $7.02 \times 10^{-6} \text{ Am}^2$, magnetic coercivity of -925 and +800 Oe, and a magnetic remanence of $3.01 \times 10^{-6} \text{ Am}^2$. The increase in coercivity for the gold-coated particles is reasonable since the gold shell prevents oxidation of the iron core resulting in a larger magnetic moment in the presence of the applied field. Previous characterization of gold-coated iron particles indicates that below the blocking temperature for Fe@Au nanoparticles, 42 Kelvin, the particles display ferromagnetic properties and following magnetization retain residual magnetism in the absence of the external magnetic field. Based on the results shown below, it can be seen that the Fe@Au NP's do display such characteristics. Above the blocking temperature the particles display superparamagnetic properties, and have a net magnetic moment of zero after magnetization.

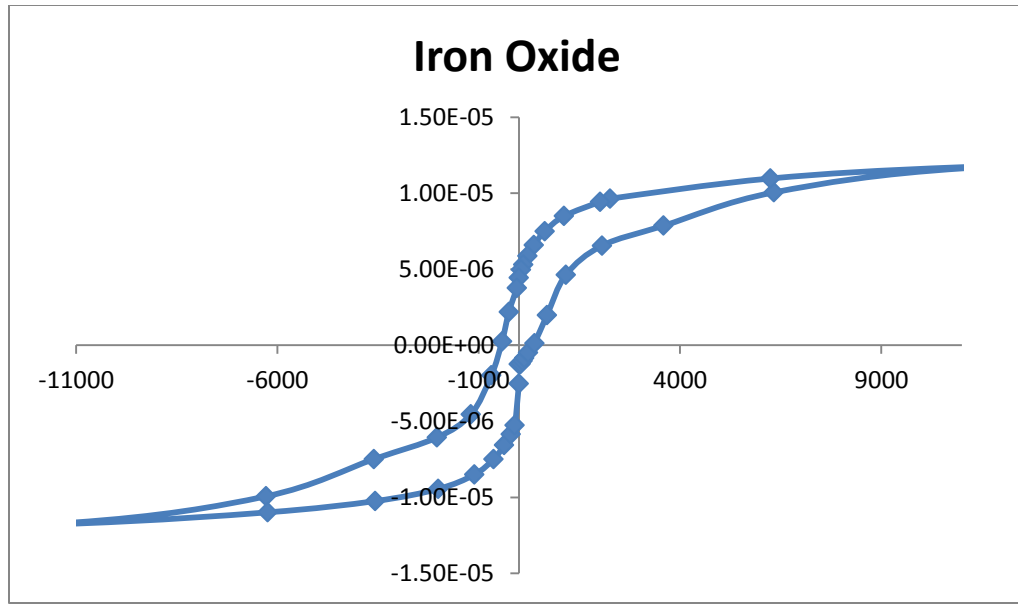


Figure 15: Magnetic Hysteresis Loop of Iron Oxide Product. Hysteresis loop for iron oxide particles obtained at 10 K. The values for the x-axis are in Oersteds (Oe), and the values for the y-axis are in units of Am^2 (Amps/meter²)

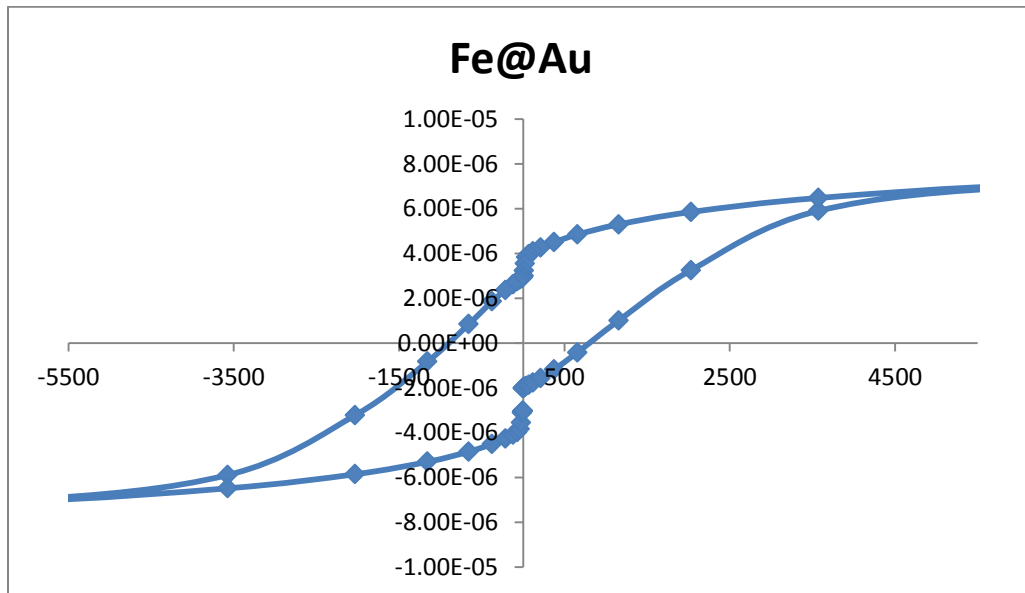


Figure 16: Magnetic Hysteresis Loop of Fe@Au Product. Hysteresis loop for Fe@Au particles obtained at 10 K. The values for the x-axis are in Oersteds (Oe), and the values for the y-axis are in units of Am^2 (Amps/meter²)

TGA Trials

Evaluating the trend of sample weight for these nanoparticles over an increasing temperature range can give invaluable information regarding the percentage of surfactant or stabilizing agent present on the particle surface, and indicate if a phase change or oxidation has occurred. Three trends are shown below in Figures 17, 18, and 19. The first plot shows the change of sample weight of the Fe@Au product. The total percent weight lost is 9.5 % of the sample mass. The second spectrum shown is from the sample containing gold coated iron nanoparticles treated with the surface-stabilizing agent carboxy thiol polyethylene glycol. A 6.5% weight change occurs at 150 °C, but appears to be a slower process than heating the untreated sample. The decomposition is completed around 400 °C (Figure 19). At 500 °C, an increase in weight is seen for about a 4% increase in sample weight. This increase was likely a result of exposed particle

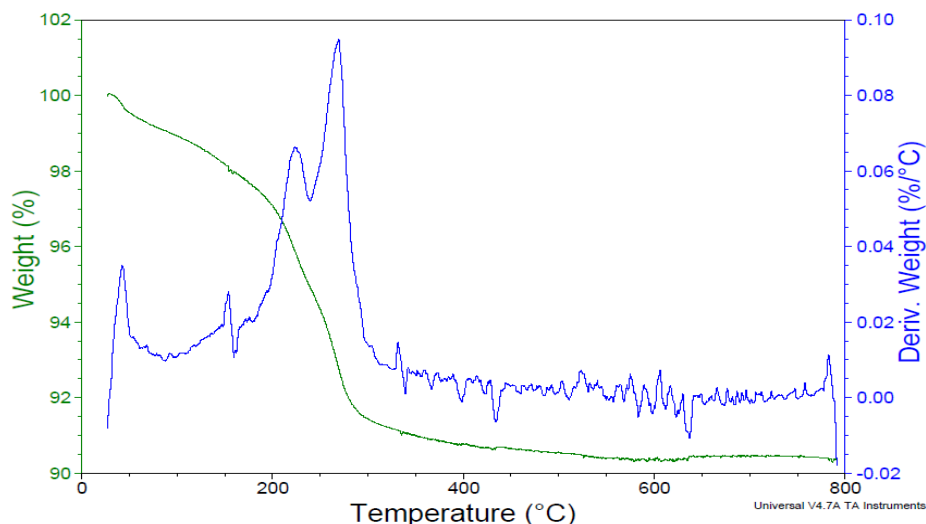


Figure 17: TGA of 20 Molar Ratio Fe@Au Product. Thermogravimetric analysis of the dried gold-coated iron nanoparticle. The green line shows the change in sample weight, while the blue line depicts the 1st derivative of the weight change.

surfaces that weren't protected from oxidation due to non-uniform gold reduction. Figure 20 shows the weight change of the iron oxide nanoparticles that were uncoated. A weight loss similar to that seen in the first two TGA plots was observed beginning at around 200 °C, but has a high rate of loss unlike the treated gold nanoparticle sample. The increase in weight began at a higher temperature compared to the treated sample, starting at 650 °C, for a 3% weight increase.

The notable loss of weight in both the washed and raw product plots is due to the decomposition and/or evaporation of CTAB, which has a melting point of 210°C. To determine whether decomposition or evaporation are occurring and at what relative rate, additional characterization of the TGA sample off-gas would need to be performed using mass spectrometry. The approximate weight percentage lost is identical for both products.

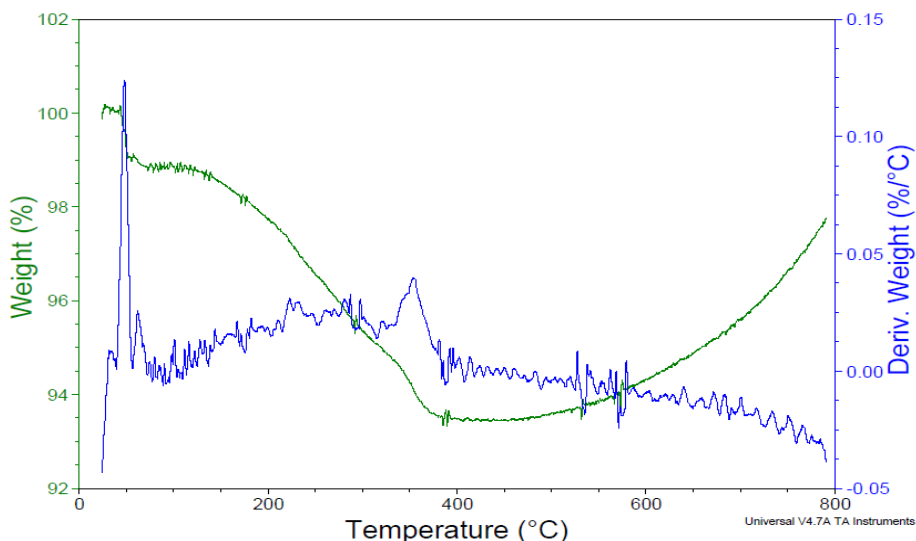


Figure 18: TGA of 20 Molar Ratio CT-Peg Fe@Au. Thermogravimetric analysis of the dried CT-Pegylated gold-coated iron nanoparticle product. The green line shows the change in sample weight, while the blue line depicts the 1st derivative of the weight change.

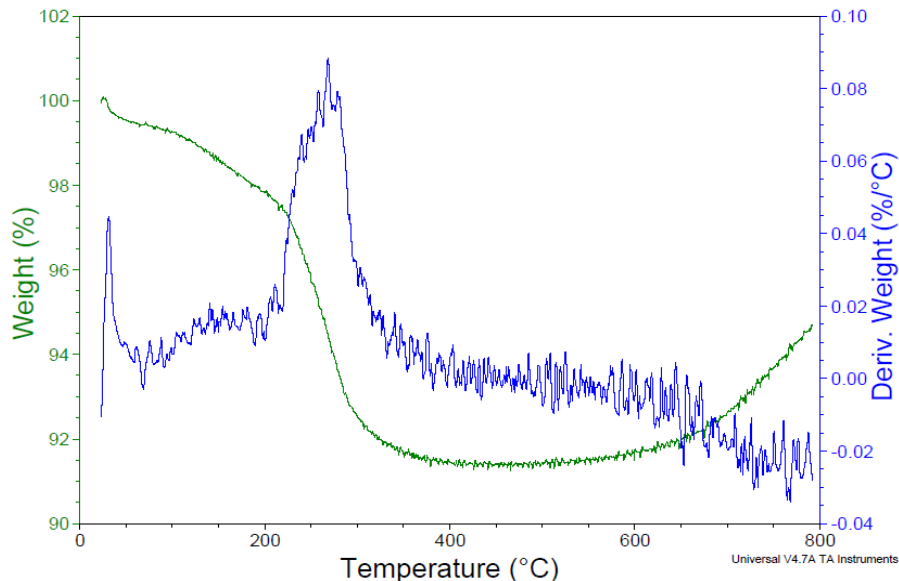


Figure 19: TGA of 20 Molar Ratio Iron Oxide Product. Thermogravimetric analysis of the dried iron oxide nanoparticle powder. The green line shows the change in sample weight, while the blue line depicts the 1st derivative of the weight change.

A NOVEL APPROACH FOR TARGETED GOLD REDUCTION

Iron Reduction of Aqueous Gold

The following results are preliminary since only colorimetric characterization had been obtained at this time. Initial reduction of the iron by sodium borohydride causes the light green mixture to turn to black as the iron is reduced from its Iron (II) oxidation state to its zerovalent metallic state (Figure 20 left). With the standard method of gold reduction, a large excess of sodium borohydride is present after the iron reduction. Additional sodium borohydride is added immediately following the introduction of the gold source (chloroauric acid) during step 3. This causes the mixture to turn to a dark purple as colloidal gold is formed in the reaction alongside the gold-coated iron



Figure 20: Image of Unoxidized and Oxidized Iron from Novel Gold Reduction Approach. An image of the iron nanoparticles immediately following reduction (left) and after the addition of chloroauric acid (right).

nanoparticles. When the minimum amount of reducing agent was used, however, the addition of the chloroauric acid caused the solution to slowly turn from black to a reddish-brown (Figure 20 right). Considering the inert environment that the reaction took place in, the only cause of this color change was the chloroauric acid in solution. This colorimetric response indicated that iron was oxidizing as gold was preferentially reduced at the iron nanoparticle surface. Reduction caused aqueous iron oxide to form and be redispersed in the solution as the entirety of the gold atoms are reduced to their zerovalent form. After removing the nanoparticles from the inert environment, there was a black product formed, and a significant amount of reddish-brown iron oxide product (Figure 31). Considering the adjustment of reducing agent used in the modified synthesis method, the amount of gold used would need to be modified to ensure that there wasn't an excess of chloroauric acid. Polavarapu *et al.* determined that a large concentration of chloroauric acid in a reducing solution can cause formation of gold nanowires as opposed to spherical gold particle formation.¹⁹ The shape of the resulting gold shell still requires characterization. The reduction of gold is initiated at the iron particle surface.

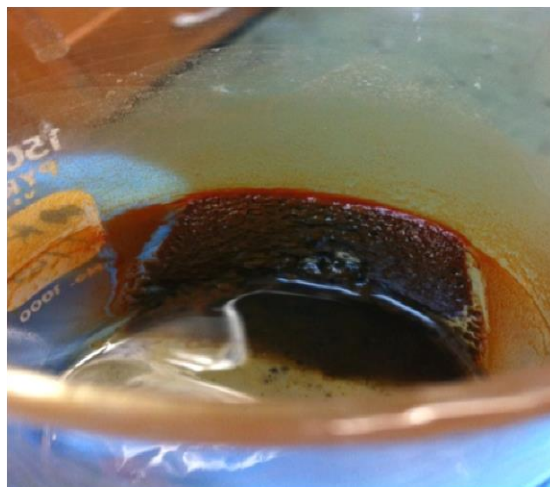


Figure 21: Image of Novel Gold Reduction Approach Product. An image of the final product of the modified synthesis immediately following completion in air.

CHAPTER V

CONCLUSIONS

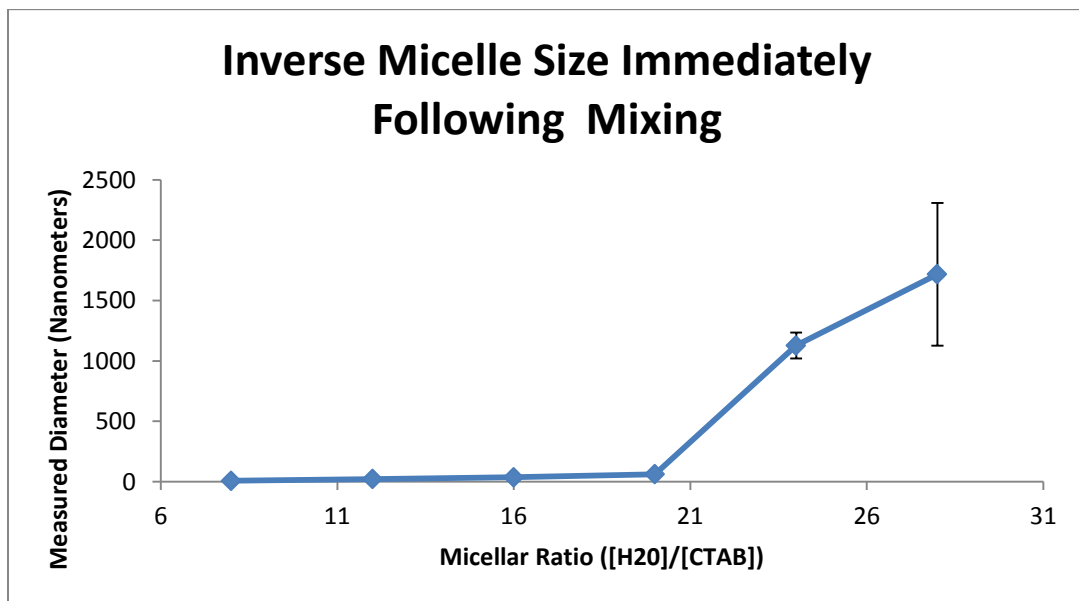
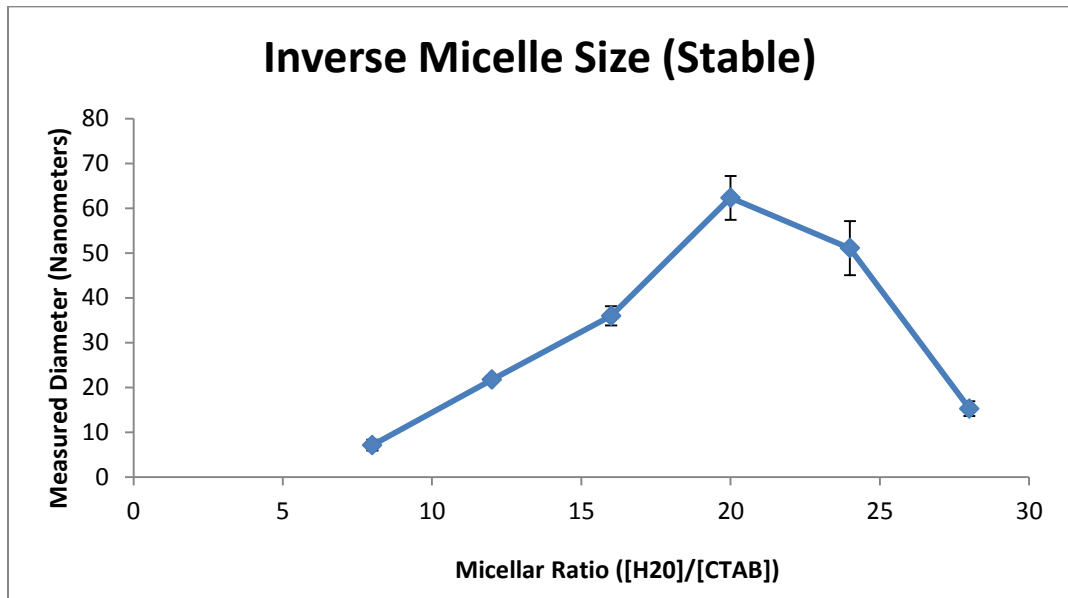
Current methods for synthesizing gold-coated magnetic nanoparticles were reviewed. The method providing the highest level of nanoparticle size and shape control was identified. This method, by Lin *et al.*, was refined by studying the effects of varying micelle size, the effects of varying the amount of reducing agent, and changing the primary source of gold reduction. The relationship of inverse micelle size versus particle size in the product provided a limited linear range, up to 75 nanometer inverse micelles. The structural integrity of the micelle becomes compromised at this ratio, leading to disassociation of the micelle and separation of the different phases. Gold-coated iron nanoparticles formed using a 20 molar ratio ranged in size from 55-95 nanometers. Light scattering analysis of this product calculated an average diameter of 126.58 nanometers. The apparent aggregation of these particles was reduced by functionalization of the gold particle surface with CT-Peg, but not eliminated. Improved particle stability and minimized aggregation is possible by incorporating stabilizing agents, such as citrate anions, immediately following gold reduction onto the iron particle surface. Magnetic properties of the products were evaluated. The important relationship between particle size and magnetic separation in solution requires definition before integration into a biosensor regiment can be enacted. Reduction of the gold can be shifted to occur at the iron particle surface and solvent interface, as opposed to spontaneous reduction within the solution. Determination of the exact ratio of iron needed to reduce the aqueous gold without causing complete oxidation of the iron nanoparticle has not yet been performed.

It is one of the first tasks to be completed for future research in this project. Significant progress was made controlling the gold-coated iron particle size, and minimizing the amount of gold necessary for large scale production of these particles. Much remains to be done before the process is “biosensor-ready”.

APPENDIX

DYNAMIC LIGHT SCATTERING

Micelle Size (Stable Values)



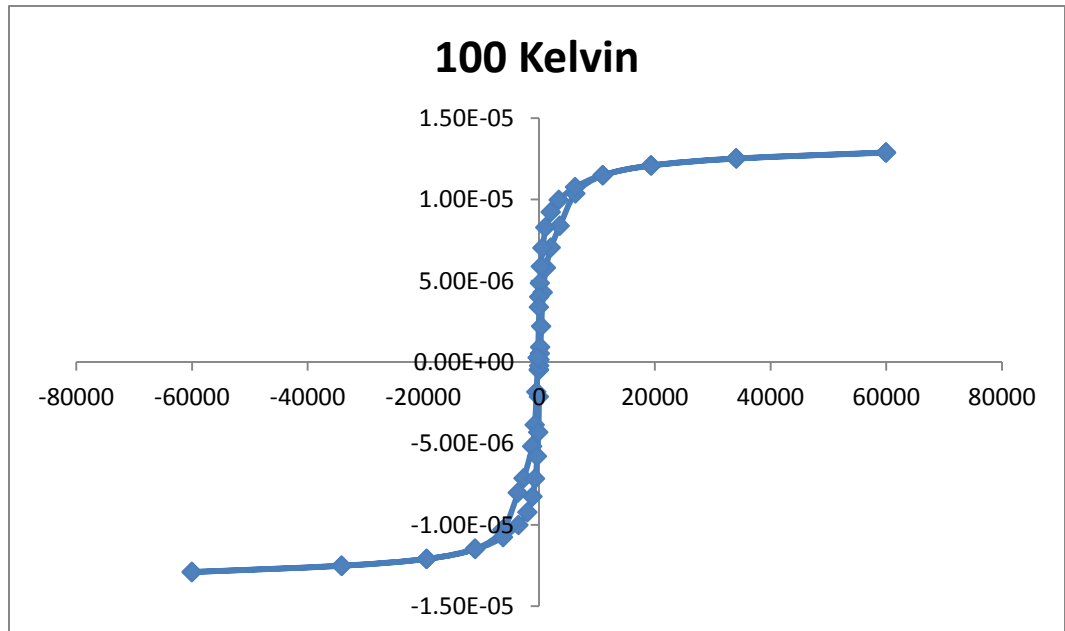
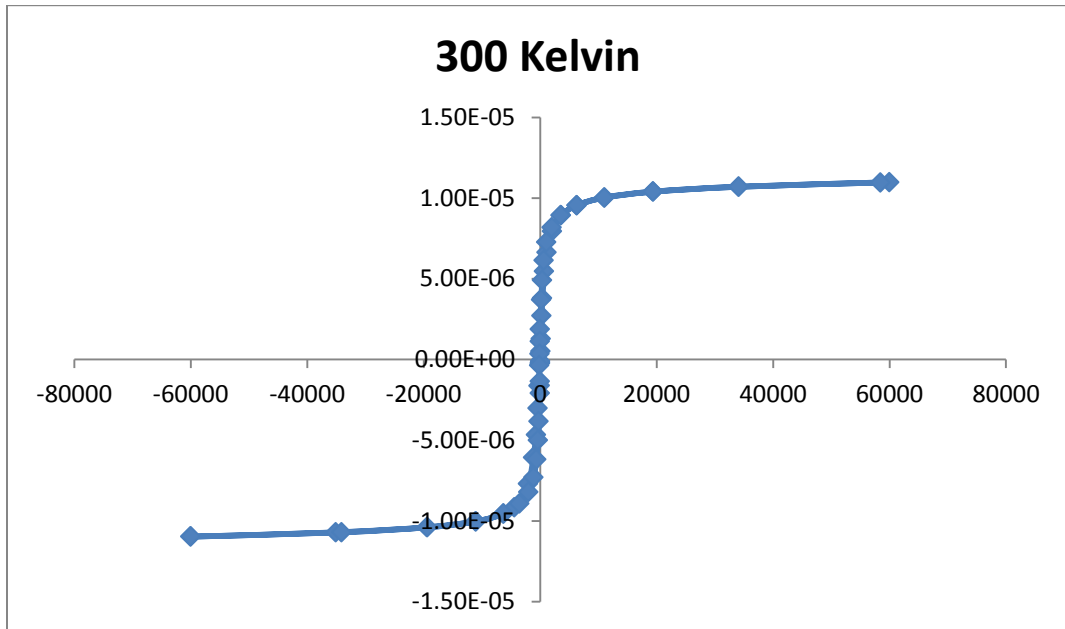
DLS DATA							
<i>Inverse Micelle</i>		8 Molar Ratio	12 Molar Ratio	16 Molar Ratio	20 Molar Ratio	24 Molar Ratio	28 Molar Ratio
Sample 1	Trial 1	9.108	21.83	26.89	62.73	51.41	Large
	Trial 2	4.981	24.24	37.03	42.23	58.2	14.18
	Trial 3	2.18	19.61	36.18	56.33	61.92	15.42
Sample 2	Trial 1	8.979	21.08	35.41	64.88	38.59	Large
	Trial 2	6.434	21.54	39.45	69.02	49.25	9.215
	Trial 3	8.363	22.14	39.46	67.75	50.51	12.71
Sample 3	Trial 1	1.678	21.35	34.79	62.15	30.89	Large
	Trial 2	13.11	22.91	37.24	67.17	58.94	23.89
	Trial 3	9.108	20.88	37.34	68.43	59.92	16.16
	Average	7.104555556	21.73111111	35.97666667	62.29888889	51.07	15.2625
	Standard Deviation	3.67164902	1.308170903	3.759986702	8.525434658	10.46149607	4.889240994
	Standard Error	1.223883007	0.755272823	2.170829335	4.922161995	6.039947572	1.629746998
Colloidal Gold							
		5 nm	10 nm	20 nm	40 nm	100nm	200 nm
Sample 1	Trial 1	12.4	20.39	32.59	52.64	113	170.4
	Trial 2	14.75	20.17	34.67	51.83	121.07	191.4
	Trial 3	13.63	20.65	30	50.96	120.7	207.9
Sample 2	Trial 1	14.64	18.07	26.97	50.07	117.6	200.9
	Trial 2	13.01	20	27.21	51.21	120.2	203.6
	Trial 3	13.55	19.97	29.25	53.71	119.2	207.9
Sample 3	Trial 1	14.18	17.74	29.22	51.46	116.8	183.9
	Trial 2	13.43	17.26	29.05	53.42	118.4	199
	Trial 3	14.2	16.02	28.93	54.39	118.1	207.7
	Average	13.75444444	18.91888889	29.76555556	52.18777778	118.3411111	196.9666667
	Standard Deviation	0.766992684	1.66829587	2.454730694	1.435964639	2.467734003	12.8714801
	Standard Error	0.255664228	0.556098623	0.818243565	0.47865488	0.822578001	4.290493367
	Absolute Error	8.754444444	8.918888889	9.765555556	12.18777778	18.34111111	3.033333333

Untreated Product Size		
Sample 1	Trial 1	103.5
	Trial 2	134.7
	Trial 3	143.8
Sample 2	Trial 1	121.2
	Trial 2	142.9
	Trial 3	159
Sample 3	Trial 1	129.3
	Trial 2	139.3
	Trial 3	152.9
	Average	136.2888889
	Standard Deviation	16.78938984
	Standard Error	5.596463279
CTPEG Product Size		
Sample 1	Trial 1	123.5
	Trial 2	122.2
	Trial 3	135.4
Sample 2	Trial 1	134.3
	Trial 2	123
	Trial 3	127.4
Sample 3	Trial 1	125.9
	Trial 2	118.8
	Trial 3	128.8
	Average	126.5888889
	Standard Deviation	5.539278934
	Standard Error	1.846426311

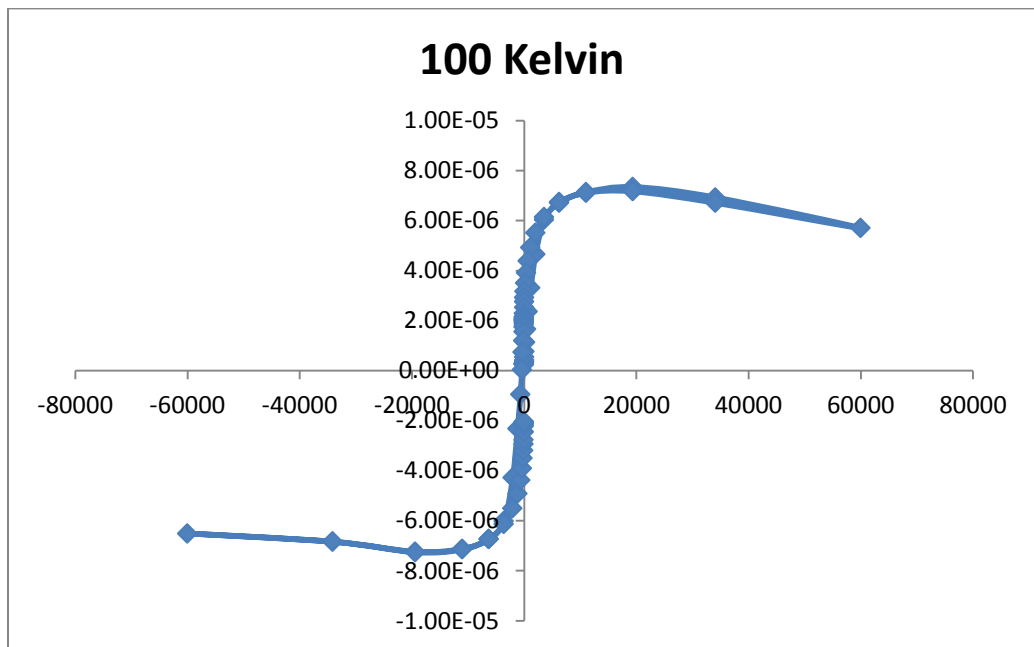
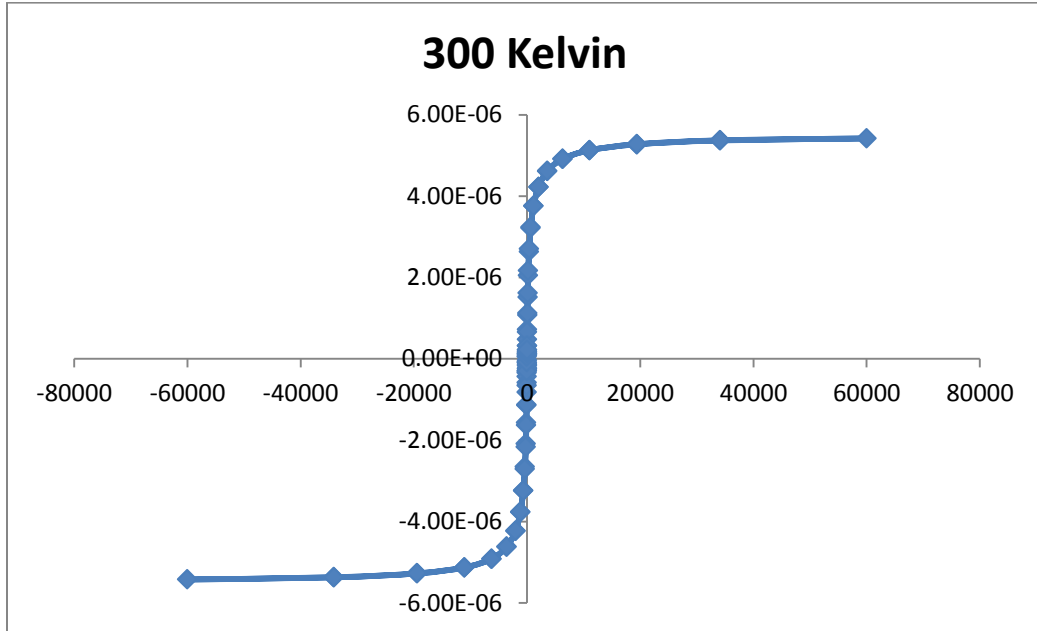
Iron Oxide NP's		
Sample 1	Trial 1	202
	Trial 2	234
	Trial 3	216.7
	Average	217.5667
	Standard Deviation	16.01759
	Standard Error	9.247762

MAGNETIC HYSTERESIS LOOPS

Iron Oxide Product

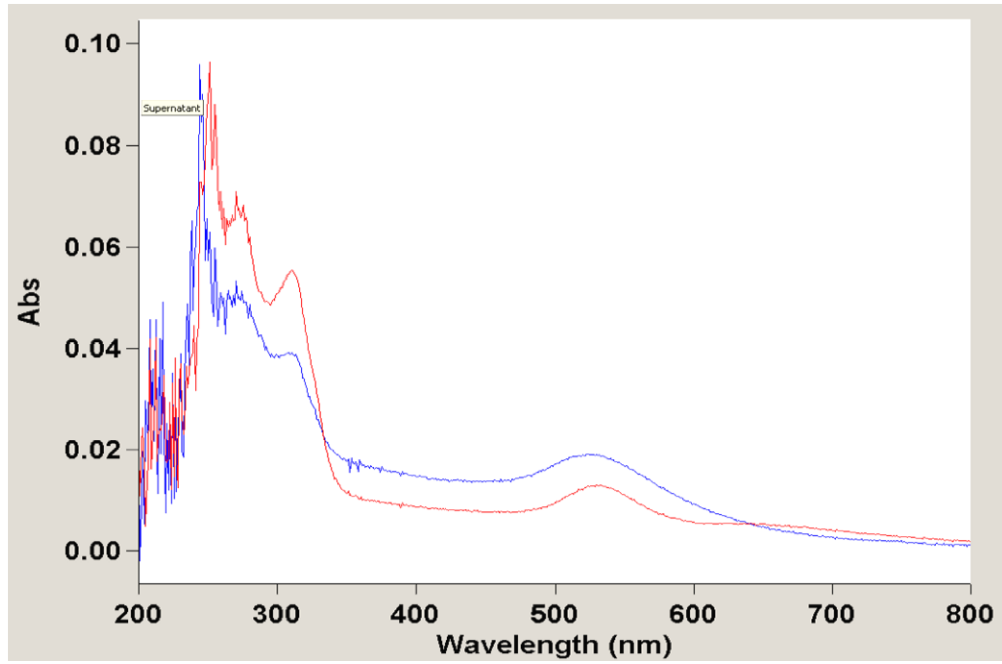


Fe@Au Product

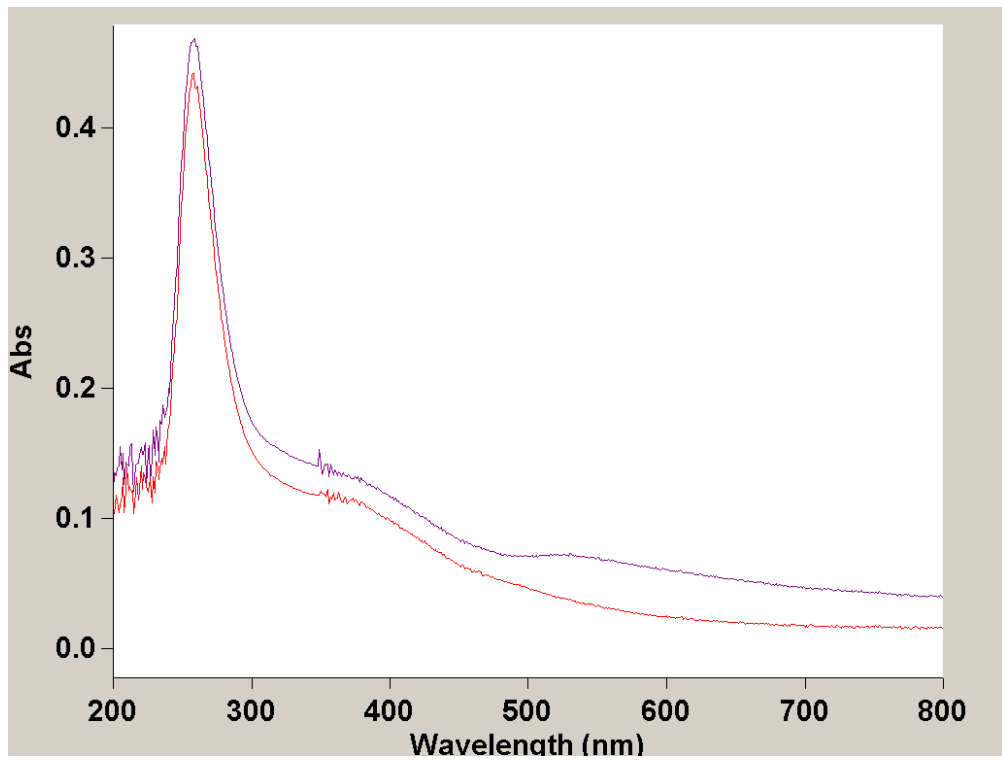


UV-VIS ABSORBANCE

Supernatant vs. Purchased Colloidal Gold



Fe@Au vs. FeO



REFERENCES

- [1] Fraga, S.; Faria, H.; Soares, M.E.; Duarte, J.A.; Soares, L.; Pereira, E.; Pereira, C.C.; Teixeira, J.P.; Bastos, M.L.; Carmo, H. Influence of the Surface Coating on the Cytotoxicity, Genotoxicity and Uptake of Gold Nanoparticles in Human HepG2 Cells. *J. of App. Tox.* **2013**, *33*, 1111-1119.
- [2] Giljohann, D.A.; Seferos, D.S.; Daniel, W.L.; Massich, M.D.; Patel, P.C.; Mirkin, C.A. Gold Nanoparticles for Biology and Medicine. *Ang. Chemie.* **2010**, *49*, 3281.
- [3] Wu, A.; Ou, P.; Zeng, L. Biomedical Applications of Magnetic Nanoparticles. *Nano.* **2010**, *5*, 246-270.
- [4] Robinson, I.; Tung, L.D.; Maenosono, S.; Walti, C.; Thanh, N.T.K. Synthesis of Core-Shell Gold Coated Magnetic Nanoparticles and Their Interaction with Thiolated DNA. *Nanoscale.* **2010**, *2*, 2624-2630.
- [5] Wagstaff, A.J.; Brown, S.D.; Holden, M.R.; Craig, G.E.; Plumb, J.A.; Brown, R.E.; Schreiter, N.; Chrzanowski, W.; Wheate, N.J. Cisplatin Drug Delivery Using Gold-Coated Iron Oxide Nanoparticles for Enhanced Tumour Targeting with External Magnetic Fields. *Inorg. Chim. Act.* **2012**, *393*, 328-333.
- [6] Lin, J.; Zhou W.; Khumbar, A.; Wiemann, J.; Fang, J.; Carpenter, E.E.; O'Connor, C.J. Gold-Coated Iron (Fe@Au) Nanoparticles: Synthesis, Characterization, and Magnetic Field-Induced Self-Assembly. *J. of Sol. Ste. Chem.* **2001**, *11*, 26.
- [7] Zhang, H.; Meyerhoff, M. Gold-Coated Magnetic Particles for Solid-Phase Immunoassays: Enhancing Immobilized Antibody Binding Efficiency and Analytical Performance. *Anal. Chem.* **2006**, *78*, 609-616.

- [8] Chen, M.; Yamamuro, S.; Farrell, D.; Majetich, S. Gold-Coated Iron Nanoparticles for Biochemical Applications. *J. of App. Phys.* **2003**, *93*, 7551-7553.
- [9] McCoy, R.S.; Choi, S.; Collins, G.; Ackerson, B.J.; Ackerson, C.J. Superatom Paramagnetism Enables Gold Nanocluster Heating in Applied Radiofrequency Fields. *ACS Nano.* **2013**, *7*, 2610-2616.
- [10] Salehizadeh, H.; Hekmatian, E.; Sadeghi, M.; Kennedy, K. Synthesis and Characterization of Core-Shell Fe₃O₄-Gold-Chitosan Nanostructure. *J. of Nanobio.* **2012**, *10*, 2-7.
- [11] Liu, B.; Zeng, H.C. Symmetric and Asymmetric Ostwald Ripening in the Fabrication of Homogeneous Core-Shell Semiconductors. *Small.* **2005**, *1*, 567.
- [12] Cho, S.J.; Idrobo, J.C.; Olamit, J.; Liu, K.; Browning, N.D.; Kauzlarich, S.M. Growth Mechanisms and Oxidative Resistance of Gold-Coated Iron Nanoparticles. *Chem. Mater.* **2005**, *17*, 3181.
- [13] Gadde, R.R.; Laitinen, H.A. Heavy Metal Adsorption by Hydrous Iron and Manganese Oxides. *Anal. Chem.* **1974**, *46*, 2023.
- [14] Boal, A.K.; Frankamp, B.L.; Uzun, O.; Tuominen, M.T.; Rotello, V.M. Modulation of Spacing and Magnetic Properties of Iron Oxide Nanoparticles through Polymer-Mediated 'Bricks and Mortar' Self-Assembly. *Chem. Mater.* **2004**, *16*, 3252-3256.
- [15] Lyon, J.L.; Fleming, D.A.; Stone, M.B.; Schiffer, P.; Williams, M.E. Synthesis of Fe Oxide Core/Au Shell Nanoparticles by Iterative Hydroxylamine Seeding. *Nano. Lett.* **2004**, *4*, 719.
- [16] Evans, D.F. The Determination of the Paramagnetic Susceptibility of Substances in Solution by Nuclear Magnetic Resonance. *J. Chem. Soc.* **1959**, 2003-2005.

- [17] Schnabel, U.; Fischer, C.H.; Kenndler, E. Characterization of Colloidal Gold Nanoparticles According to Size by Capillary Zone Electrophoresis. *J. Microcol. Sep.* **1997**, *9*, 529.
- [18] Raegan, A.N.; Reiter, K.; Dion, A.; Clarke, A.J.; Lipkowski, J.; Dutcher, J.R. Advances in Surface Plasmon Resonance Imaging Enable Quantitative Tracking of Nanoscale Changes in Thickness and Roughness. *Anal. Chem.* **2014**, *86*, 3346.
- [19] Polovarapu, L.; Venkatram, N.; Ji, W.; Xu, Q.H. Optical-Limiting Properties of Oleylamine-Capped Gold Nanoparticles for Both Femtosecond and Nanosecond Laser Pulses. *ACS App. Mater. Interfaces.* **2009**, *10*, 2299.